Graphene-Based Materials for Hydrogen Generation from Light-Driven Water Splitting

ARTICLE *in* ADVANCED MATERIALS · JULY 2013

Impact Factor: 17.49 · DOI: 10.1002/adma.201301207 · Source: PubMed

6 AUTHORS, INCLUDING:

Guancai Xie
Chongqing University
3 PUBLICATIONS **148** CITATIONS
SEE PROFILE

Kai Zhang
National Center for Nanoscience and Tech…
12 PUBLICATIONS **549** CITATIONS
SEE PROFILE

Beidou Guo
National Center for Nanoscience and Tech…
7 PUBLICATIONS **1,430** CITATIONS
SEE PROFILE

Jian-Ru Gong
National Center for Nanoscience and Tech…
39 PUBLICATIONS **2,528** CITATIONS
SEE PROFILE

Graphene-Based Materials for Hydrogen Generation from Light-Driven Water Splitting

*Guancai Xie, Kai Zhang, Beidou Guo, Qian Liu, Liang Fang, and Jian Ru Gong**

Dedicated to Professor Chunli Bai on the occasion of his 60th birthday

Hydrogen production from solar water splitting has been considered as an ultimate solution to the energy and environmental issues. Over the past few years, graphene has made great contribution to improving the light-driven hydrogen generation performance. This article provides a comprehensive overview of the recent research progress on graphene-based materials for hydrogen evolution from light-driven water splitting. It begins with a brief introduction of the current status and basic principles of hydrogen generation from solar water splitting, and tailoring properties of graphene for application in this area. Then, the roles of graphene in hydrogen generation reaction, including an electron acceptor and transporter, a cocatalyst, a photocatalyst, and a photosensitizer, are elaborated respectively. After that, the comparison between graphene and other carbon materials in solar water splitting is made. Last, this review is concluded with remarks on some challenges and perspectives in this emerging field.

1. Introduction

Global energy demand for a sustainable development will double by 2050. Nowadays, energy crisis and environmental contamination are serious issues and thus seeking for renewable and clean energy is an urgent task. Solar energy has been considered as an ideal alternative, since it is the most powerful, affordable (cost-free) and richest renewable and sustainable source of energy.[1] The economical conversion of solar energy into chemical fuels is one of the Holy Grails of 21st century science. Hydrogen (H_2) is predicted to be a promising secondary energy, with the advantages of high energy density (140 MJ Kg^{-1}) which far exceeds those of gasoline and coal, no carbon emission, and a useful by-product of water from combustion.[2] At present, hydrogen is mainly produced from fossil fuels such as natural gas by steam reforming which is severely restricted by its low efficiency and high cost. Moreover, carbon dioxide is emitted in this process. As is known, nature abundantly stores hydrogen in the form of water. Therefore, hydrogen production by efficient combination of water and solar energy has enormous capacity to fulfill the present and future demand of energy around the world in an eco-friendly manner.

There are several methods for utilizing solar radiation in splitting water for hydrogen generation.[2,3] However, photovoltaic electrolysis of water uses the expensive proton exchange membranes[4] and alkaline electrolytes.[5] Solar to thermochemical water splitting needs the high temperature of 700–1000 °C.[6] Photobiological water splitting has to overcome the natural short-term nature of biospecies hydrogen production.[7] Consequently, much attention has been focused on water splitting for hydrogen generation by photoelectrochemical (PEC) or photocatalytic reactions because they are cost-effective, simple and convenient, and have huge potential for further development.[8]

In 1972, Honda and Fujishima reported that H_2 evolution could be observed on a TiO_2 electrode under UV-light irradiation in a PEC cell with Pt counter electrode.[9] It was the first demonstration that hydrogen could be obtained through water splitting using PEC method. Afterwards, the principle of PEC hydrogen production was successfully extended into particulate system for heterogeneous photocatalysis by Allen J. Bard.[10] During the past 50 years, great progress has been made in this rapidly growing field.[8,11] As the earliest H_2 production semiconductor, TiO_2 is the most investigated photoelectrode/photocatalyst material due to its high-efficiency, low-cost, non-toxicity, and photostablility.[12] Metal oxides with ABO_3 configuration, such as $SrTiO_3$,[13] $NaTaO_3$,[14] perfectly meeting the thermodynamic requirement for water splitting, are also reported to be efficient photocatalysts. But all of them are only active under UV-light, which accounts for about 4% of the total solar spectrum. Therefore, it is necessary to design efficient photoelectrodes or photocatalysts with visible-light response (~43% of solar spectrum), in order to sufficiently utilize solar energy. Recently, oxysulphides and (oxy)nitrides, which possess relatively narrow bandgaps, are reported to be effective for H_2 production by Domen group.[15] Especially, $(Ga_{1-x}Zn_x)(N_{1-x}O_x)$ is proved to be the most efficient photocatalyst capable of splitting pure water under visible-light irradiation.[16] Metal sulphides, e.g. Pt/PdS/CdS,[17] are also efficient semiconductor materials for PEC or photocatalytic H_2 production due to their suitable bandgaps and high conduction

G. Xie, Dr. K. Zhang, B. Guo, Q. Liu, Prof. J. R. Gong
National Center for Nanoscience and Technology
11 Zhongguancun Beiyitiao
Beijng 100190, People's Republic of China
E-mail: gongjr@nanoctr.cn
G. Xie, Prof. L. Fang
Department of Applied Physics
Chongqing University
Chongqing 400044, People's Republic of China

DOI: 10.1002/adma.201301207

bands, although sacrificial reagents are always needed to consume the photogenerated holes.[18] In addition, PEC cells with various novel configurations are constructed for water splitting.[19] For example, Licht et al. presented the concept of multiple bandgap tandem cells and demonstrated a PEC solar-to-hydrogen (STH) efficiency of 18.3% using illuminated AlGaAs/Si and RuO_2/Pt photoelectrodes, and also reported conversion efficiencies of up to 19.6% for multijunction regenerative cells.[19a,b] However, several key factors such as low light absorption, rapid charge recombination, and instability of semiconductor materials during chemical process are still big challenges for this "dreaming technology", which restrict the realization of large-scale industrial application.[20]

The emergence of nanomaterials as the new building blocks to construct light energy harvesting assemblies has opened up new ways to utilize renewable energy resources because of large surface areas, abundant surface states, and diverse morphologies compared to their corresponding bulk materials.[11,21] Among them, graphene, a two-dimensional (2D) network of hexagonal structured sp^2-hybridized carbon atoms,[22] has stimulated tremendous research interest in various energy conversion applications.[23] Graphene exhibits many outstanding properties, such as fast room-temperature mobility of charge carriers (200000 $cm^2 V^{-1} s^{-1}$), exceptional conductivity (10^6 S cm^{-1}), large theoretical specific surface area (2630 $m^2 g^{-1}$), and excellent optical transmittance (~97.7%).[24] These unique properties indicate that graphene has great potential to be an ideal construction component of PEC electrodes or photocatalytic materials for hydrogen production.

Due to the rapid growth in the technologies for preparation of graphene or its derivates, investigations on the graphene-based nanomaterials for applications in the PEC and photocatalytic hydrogen production field are also under fast-paced development, and many encouraging findings have been made in the past several years.[25] Therefore, making a comprehensive review in this specific field is of great theoretical and practical necessary at the present stage.

In this article, we overview the recent development on graphene-based materials for photoelectrochemical and photocatalytic hydrogen generation from water splitting. After a brief introduction of the basic principles of solar water splitting and the tailored properties of graphene for this application, the roles of graphene in hydrogen generation reaction, including an electron acceptor and transporter, a cocatalyst, a photocatalyst, and a photosensitizer, are elaborated respectively. Then, the comparison between graphene and other carbon materials in the PEC/photocatalytic application is presented. Last, the challenges and perspectives in this emerging field are discussed. This paper will provide important scientific reference on applying graphene to water splitting for realizing large-scale hydrogen generation in the near future.

2. Principles of PEC and Photocatalytic H_2 Generation

The standard Gibbs free energy change for the splitting of H_2O into H_2 and O_2 is + 237.2 kJ mol^{-1} according to Equation 1, which corresponds to 1.23 eV per electron transferred.[11a] Thus, for overall water splitting into H_2 and O_2 simultaneously, it is necessary to have a semiconductor with a bandgap larger than 1.23 eV, along with suitable band edge positions that well straddle water-splitting potential. That is, the bottom of conduction band (CB) has to be more negative than the redox potential of H^+/H_2 (0 V vs NHE (normal hydrogen electrode), pH = 0), while the top of valence band (VB) more positive than the redox potential of O_2/H_2O (1.23 V). Here, we will present two approaches for H_2 generation from light-driven water splitting, namely, PEC and photocatalytic H_2 generation.

$$H_2O_{(l)} \rightarrow H_{2(g)} + \frac{1}{2}O_{2(g)},\ \Delta G = +237.2\,\text{kJ mol}^{-1} \quad (1)$$

As illustrated in **Scheme 1**a, PEC H_2 generation is carried out in a PEC cell under light irradiation, which consists of a working photoanode (photoactive materials) for O_2 evolution, a counter photocathode (such as Pt) for H_2 evolution, and an electrolyte solution as well as a wire completing the current loop between the photoelectrodes and the external circuit. Actually, very few semiconductor materials satisfy the necessary requirements for both water oxidation and reduction and for good electrode stability in aqueous electrolyte solutions simultaneously. Fortunately, a semiconductor with a bandgap less than 1.23 eV or a CB bottom level mismatching the reduction potential of H^+/H_2 can also be applied for H_2 production, such as p-Si and Fe_2O_3 photoelectrodes,[26] because an external bias can provide

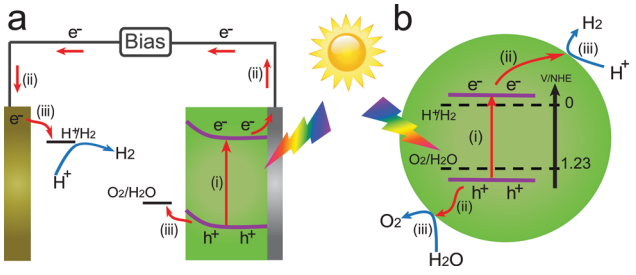

Scheme 1. The principle and main process of a) photoelectrochemical and b) photocatalytic hydrogen generation from water splitting.

Jian Ru Gong is a professor at National Center for Nanoscience and Technology, China. She received her Ph.D in Physical Chemistry from Institute of Chemistry, Chinese Academy of Sciences under the guidance of Prof. Chunli Bai (2005), and was a postdoctoral fellow with Prof. Charles M. Lieber at Harvard University (2005-2008). Her research interest focuses on design and preparation of novel nanomaterials and devices, and their applications in energy and biomedicine. See http://www.nanoctr.cn/gongjianru for details.

Adv. Mater. 2013,
DOI: 10.1002/adma.201301207

an additional energy input to enable the reaction at the counter electrode, while the employment of an electrical bias is undesirable for technological applications. An additional role of the bias is to allow a partial depletion of electrons in the photoactive materials. This electron depletion corresponds to the formation of the surface space charge layer and the associated bending bands, which can reduce recombination and increase the life time of photogenerated charges, thereby improving the H_2-production activity.[27] The reaction mechanism is described in the following half-cell reactions:

$$2H^+ + 2e^- \rightarrow H_2(\text{photocathode}) \quad (2)$$

$$H_2O \rightarrow \frac{1}{2}O_2 + 2H^+ + 2e^-(\text{photoanode}) \quad (3)$$

Different from PEC H_2 generation, photocatalytic H_2 generation is carried out in a suspension system using particulate semiconductor photocatalysts excited by photons, as illustrated in Scheme 1b. Similarly, the number of reliable and stable photocatalysts capable of overall water splitting is limited due to the stringent requirements, which are essentially the same as PEC water splitting with no external bias applied. For such a system, a semiconductor with a relative negative CB bottom level compared to the reduction potential of H^+/H_2 is required for solar H_2 generation. In most cases, photocatalytic H_2 generation is carried out in aqueous solution containing electron donors as sacrificial reagents such as alcohols, lactic acid, and S^{2-}/SO_3^{2-}, which can irreversibly consume the photogenerated holes and suppress the recombination of electrons and holes in the semiconductor photocatalyst, thus enhancing the H_2 generation rate and improving the photocatalytic stability.[11a] The reaction in the presence of sacrificial reagents is often regarded as a half reaction of water splitting and the mechanism can be briefly described as follows:

$$\text{Red} + H_2O \xrightarrow{h\nu,\text{photocatalyst}} \text{Ox} + H_2 \quad (4)$$

where Red represents the electron donor, and Ox the product by hole oxidation.

The main process in generation of H_2 for both approaches is similar, and it includes three basic steps: (i) the photocatalyst absorbs photons to form electron-hole pairs in the material; (ii) the photoinduced charges separate and migrate to different sites of the photocatalyst; and (iii) water is reduced by photogenerated electrons to evolve H_2 on the surface of the counter electrode in the case of the PEC system, or on the surface of the photocatalyst in the case of the photocatalytic system, as shown in Scheme 1. The rate of H_2 evolution is commonly dominated by the amount of excited electrons that survive to reduce protons. Thus, an efficient photoelectrode or photocatalyst should first have a suitable band structure to allow for abundant absorption overlap with the solar spectrum. Meanwhile, the excited charges should be separated and transported to the surface of the photoelectrode or photocatalyst efficiently, instead of producing heat via the electron-phonon interaction, recombining via inter-band transition, or trapping by bulk or surface recombination centers. Finally, the semiconductor should have enough reactive sites for efficient utilization of the photogenerated charges, or the desired reactions can be promoted by the presence of a solid cocatalyst, and the back reaction to form water should be retarded. In addition, the photoactive materials should be stable during the PEC or photocatalytic reactions to ensure the long-term duration of the system.

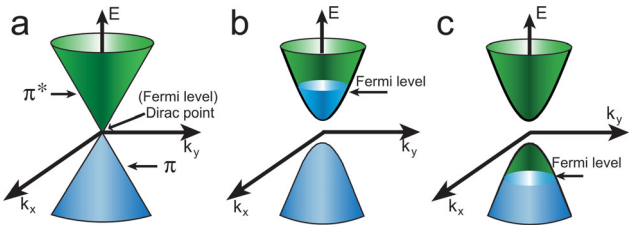

Scheme 2. a) Approximation of the low energy band structure of pristine graphene with two cones touching at a Dirac point; energy band structure of b) n-type and c) p-type graphene with a bandgap.

3. Tailoring Properties of Graphene for PEC/Photocatalytic H_2 Generation

Graphene is usually described as a zero bandgap semiconductor. Fundamentally, the π^*-state conduction band and the π-state valence band of graphene touch each other at the Dirac point,[28] as illustrated in **Scheme 2**a. The band structure of graphene is symmetric about the Dirac point with the Fermi level located between VB and CB. As a result, the low-energy dispersion relation is linear and electrons in graphene behave as zero-mass Dirac Fermions with a very fast velocity of 10^6 m s^{-1}.[29] The unique band structure makes graphene display amazingly high conductivity and electron mobility. Furthermore, the band structure of graphene can be tailored by heteroatom doping or electrostatic field tuning, which usually makes graphene an n-type or p-type semiconductor with a small bandgap by detuning away the Fermi level from the Dirac point (Scheme 2b and 2c).[30] Apart from the unique electronic properties, graphene can also absorb light uniformly over a wide range of wavelength from infrared through visible to ultraviolet region, since graphene can also be regarded as a large aromatic macromolecule without a bandgap.[31]

The chemical functionalization of graphene offers an alternative approach to tuning its electronic properties.[32] For example, graphene can be p-doped or n-doped by chemical doping with electron-withdrawing oxygen functionalities or electron-donating nitrogen functionalities, respectively.[33] More importantly, functionalized graphene might be a potential candidate of non-metal semiconductor photocatalysts. Of particular interest is graphene oxide (GO), which is typically produced by chemical exfoliation of graphite through strong oxidization[34] and widely considered as an individual sheet of graphene decorated with various oxygen-containing functional groups (such as hydroxyl, epoxy, and carboxyl) on both the basal plane and the edge.[35] Compared to quasi-metallic pristine graphene, GO is an insulator due to the formation of sp^3-hybridized carbon atoms which disrupt the delocalized π-conjugation in graphene. The intrinsic structural and electronic properties of graphene can be partially restored upon reduction of GO.[36] The reduced graphene oxide (RGO), in which aromatic sp^2 domains with

few nanometers are surrounded by sp^3-hybridized carbon atoms, usually shows p-type semiconducting behavior.[37] In principle, a tunable bandgap from insulating to conducting can be achieved by controlling the reduction degree of RGO, as the bandgap energy is strongly correlated to the number of oxidized sites and oxidization degree of RGO.[38] For instance, the results from first-principles calculations[39] and controllable reduction processes[38c] suggest that a bandgap ranging from a few tenths to 4 eV can be obtained by changing the reduction level and the location of the oxidized region of RGO. It has also been demonstrated that the CB minimum of RGO is composed of anti-bonding π^* orbital, which has a higher energy level than that needed for H_2 generation.[40] Therefore, RGO alone with suitable reduction degree is likely to generate H_2 from solar water splitting.

Additionally, functionalized graphene is a promising precursor for efficient synthesis of graphene-based nanomaterials. The availability of solution-processable GO allows for the chemical modification of graphene with various molecules or nanoparticles via non-covalent or covalent functionalization.[34,41] Furthermore, GO can not only mediate the growth of nanomaterials, but also help the growth of nanomaterials with good dispersion behavior, because the presence of functional groups on GO sheets can serve as the nucleation sites to anchor nanoparticles. During the synthetic process, GO can be reduced to RGO in chemical or thermal conditions, leading to formation of RGO-based composites. For example, Dai group[42] reported a MoS_2/RGO hybrid with nanoscopic MoS_2 structures selectively grown on RGO sheets, in strong contrast to large aggregated MoS_2 nanoparticles in the absence of RGO, as shown in **Figure 1**a and Figure 1b, respectively. Li et al.[43] showed that the 2D platform structure of RGO favored the dispersion of CdS nanoparticles, which could be clearly seen from Figure 1c and Figure 1d. Obviously, RGO provides an ideal substrate to avoid agglomeration of nanoparticles, increasing the total specific surface area of the obtained graphene-based composite, which benefits the PEC/photocatalytic H_2-generation activity. Besides, the residual functional groups in RGO can improve

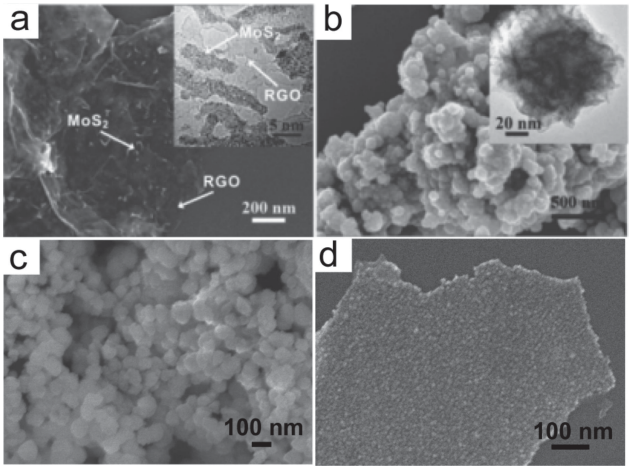

Figure 1. SEM and (inset) TEM images of a) the MoS_2/RGO hybrid and b) the free MoS_2 particles; SEM images of c) pure CdS and d) 1 wt%-RGO/CdS nanocomposites samples. Reprinted with permission.[42,43] Copyright 2011, American Chemical Society.

the solubility of graphene-based nanomaterials in water, which is a prerequisite for the H_2generation occurring in aqueous solution.

In short, graphene possesses remarkable advantages for solar H_2 generation from water splitting. First, graphene could serve as an ideal electron sink and/or electron transport bridge to facilitate charges separation in PEC/photocatalytic reaction owing to its high work function and good conductivity. Second, graphene could be a cocatalyst to substitute the commonly-used noble metal cocatalyst, because the reduction potential of graphene/graphene $^{\bullet-}$ is more negative than the reduction potential of H^+/H_2.[44] Third, functionalized graphene with a suitable oxidation level might be a photoactive material for H_2 generation. Fourth, graphene as an aromatic macromolecule or after bandgap tuning may act as a photosensitizer to extend absorption of light.

It is not surprising, therefore, numerous approaches have been developed to synthesize various graphene-based nanomaterials, and significant progress has been made on photocatalytic and PEC H_2 generation from water splitting,[45,25] as summarized in **Table 1** and **Table 2**, respectively. In the subsequent sections, different roles of graphene including an electron acceptor and transporter, a cocatalyst, a photocatalyst, and a photosensitizer for PEC and photocatalytic H_2 generation will be discussed in detail. Since all the reduction approaches allow only partial restoration of the sp^2 network, the reduced/functionalized graphene is referred to as RGO instead of graphene or GO in the composite photocatalysts for the related specific experiments in this review to avoid unnecessary confusion.

4. Graphene as an Electron Acceptor and Transporter

Due to its high work function (4.42 eV),[86] graphene can accept photogenerated electrons from the CBs of most semiconductors or the lowest unoccupied molecular orbitals (LUMOs) of dyes with no barrier, which will efficiently suppress the recombination of photogenerated charges and significantly enhance their PEC/photocatalytic H_2-production activity. Furthermore, graphene possesses extremely high conductivity, so the accepted electrons can migrate rapidly across its 2D plane to reactive sites for H_2 evolution. Therefore, the role of graphene as an electron acceptor and transporter has been extensively investigated to enhance the PEC/photocatalytic H_2-production activity recently, and many encouraging findings are already obtained in both UV- and visible light-active systems.

4.1. Graphene-Based UV-Active System

A variety of wide bandgap semiconductors have been combined with graphene for photocatalytic reactions under UV-light irradiation, such as TiO_2,[87] ZnO,[88] ZnS,[89] 6H-SiC,[90] and BiOCl.[91] Among them, only TiO_2/graphene photocatalyst was hitherto reported for photocatalytic H_2 generation.

It was reported that RGO could trap electrons from UV-irradiated TiO_2 via a percolation mechanism and transport the trapped electrons to reduce silver ion into silver

DOI: 10.1002/adma.201301207

Table 1. Graphene-based photocatalysts for H_2 production by water splitting.

Photocatalyst	Graphene content [wt%]	Preparation method	Incident light (source)[a)]	Reactant solution	H_2 evolution				Ref. (year)
					Cocatalyst	Activity [μmol h^{-1}]	Quantum yield [%]	Stability	
TiO_2/RGO	N/A	Sol-gel	UV-visible (Xe)	Na_2S, Na_2SO_3	None	8.6	N/A	N/A	[46a] (2009)
TiO_2/RGO	N/A	Hydrothermal	UV (Xe)	Na_2S, Na_2SO_3	None	20	N/A	N/A	[46b] (2011)
TiO_2/RGO	N/A	Self-assembly	UV-visible (Xe)	Methanol	None	~16	N/A	N/A	[46c] (2011)
TiO_2/RGO	2	Hydrothermal	UV-visible (Xe)	Na_2S, Na_2SO_3	None	5.4	N/A	N/A	[47b] (2012)
TiO_2/RGO	5	Sol-gel	UV-visible (Xe)	Na_2S, Na_2SO_3	None	8.6	N/A	N/A	[47a] (2010)
P25/RGO	1/6	Hydrothermal	UV-visible (Xe)	Methanol	None	74	N/A	>12 h	[48] (2011)
TiO_2/RGO	0.7	Solution mixing	$\lambda > 320$ nm (Xe)	Methanol	Pt	50	N/A	N/A	[49] (2012)
CdS/RGO	1	Solvothermal	$\lambda > 420$ nm (Xe)	Lactic acid	Pt	1120	22.5 (420 nm)	N/A	[43] (2011)
N-TiO_2/RGO	N/A	Hydrothermal	UV (Hg) Visible (Xe)	Methanol	None	716 (UV)112 (Visible)	N/A	N/A	[50] (2012)
RGO/CdS	N/A	Two-phase	~365 nm (Hg)	Methanol	Pt	5500	N/A	>16 h	[51b] (2012)
RGO/CdS	5	Precipitation	$\lambda \geq 420$ nm (Xe)	Na_2S, Na_2SO_3	None	314	N/A	>15 h	[51a] (2012)
CdS/RGO	1	Hydrothermal	$\lambda \geq 420$ nm (Xe)	Na_2S, Na_2SO_3	None	70	N/A	>15 h	[52] (2012)
SiC/RGO	1	Solution mixing	$\lambda \geq 420$ nm (Xe)	KI	None	95 (μl/h)	N/A	N/A	[53] (2013)
$ZnIn_2S_4$/RGO	5	Solvothermal	$\lambda > 420$ nm (Xe)	Na_2S, Na_2SO_3	None	81.6	N/A	>12 h	[54] (2013)
$Sr_2Ta_2O_{7-x}N_x$/RGO	5	Photoreduction	UV-visible (Xe)	Methanol	Pt	293	6.45 (280–550 nm)	N/A	[55] (2011)
C_3N_4/RGO	1	Impregnation-chemical reduction	$\lambda > 400$ nm (Xe)	Methanol	Pt	451	2.6 (>400 nm)	>12 h	[56] (2011)
$TiSi_2$/RGO	1	Precipitation	$\lambda \geq 420$ nm (Xe)	Pure water	RuO_2	97.5	N/A	>25 h	[57] (2012)
EY-RGO	3/13	in situ photoreduction	$\lambda \geq 420$ nm (Xe)	TEOA	Pt	10.17	9.3 (520 nm)	<25 h	[58] (2011)
RB-RGO	N/A	Solution mixing	$\lambda \geq 420$ nm (TH)	TEOA	Pt	14.2	18.5 (550 nm)	>44 h	[59] (2012)
EY/RB-RGO	N/A	in situ photoreduction	$\lambda \geq 420$ nm (TH)	TEOA	Pt	36.7	37.3 (520 and 550 nm)	>62 h	[60] (2012)
EY-RGO	50	Solution mixing	$\lambda > 320$ nm (Xe) $\lambda > 420$ nm (Xe)	TEOA	None	3350(UV-vis)400(vis)	N/A	>30 h	[61] (2011)
TPA-RGO	N/A	Solution mixing	UV-visible (Xe)	KI	Pt	2.3	0.45	>30 h	[62] (2012)
Ru(dcbpy)$_3$-RGO	N/A	Solution mixing	UV-visible (Xe) Visible (Xe)	TEOA	Pt	2533(uv) 118(vis)	4.89	>30 h	[63] (2012)
Ru/$SrTiO_3$:Rh/RGO/$BiVO_4$	5	Photoreduction	$\lambda > 420$ nm (Xe)	H_2SO_4	Ru	11	1.03 (420 nm)	>24 h	[64] (2011)
CTAB/TPPH-RGO	2/3	Solution mixing	UV-visible (Xe)	TEOA	Pt	2240	3.6	>15 h	[65] (2013)
CdS@TaOH-RGO	1	Hydrothermal	$\lambda > 420$ nm (Xe)	Na_2S, Na_2SO_3	Pt	633	31 (420 nm)	N/A	[66] (2012)
Cu_2O/RGO	3.8	In situ growth	$\lambda > 400$ nm (Xe)	Methanol	Pt	264.5	N/A	>15 h	[67] (2012)
TiO_2/RGO	1	Microwave-hydro-thermal	UV-visible (Xe)	Methanol	RGO	736	3.1 (365 nm)	N/A	[68] (2011)
TiO_2/RGO	2.8	Hydrothermal	UV-visible (Xe)	Methanol	None	0.29	N/A	N/A	[46d] (2012)
ZnCdS/RGO	0.25	Coprecipitation-hydrothermal	UV-visible (Xe)	Na_2S, Na_2SO_3	RGO	1824	23.4 (420 nm)	>12 h	[44] (2012)
CdS/RGO	2	Sol-gel	$\lambda > 380$ nm (Xe)	Na_2S, Na_2SO_3	RGO	~5	N/A	N/A	[69] (2012)
TiO_2/RGO	N/A	Hydrothermal	UV-visible (Xe)	Methanol	RGO	~55	N/A	N/A	[69] (2012)
TiO_2/RGO	1	Solution mixing	$\lambda > 320$ nm (Xe)	Methanol	RGO/Pt		N/A	>9 h	[70] (2011)

Table 1. Continued

Photocatalyst	Graphene content [wt%]	Preparation method	Incident light (source)[a)]	Reactant solution	H_2 evolution				Ref. (year)
					Cocatalyst	Activity [μmol h^{-1}]	Quantum yield [%]	Stability	
$CdS/Al_2O_3/RGO$	1	Solid state	Visible (TH)	Na_2S, Na_2SO_3	RGO	350	14	N/A	[71] (2012)
CdS/ZnO/RGO	1	Solid state	Visible (TH)	Na_2S, Na_2SO_3	RGO	751	30	N/A	[71] (2012)
$TiO_2/MoS_2/RGO$	5	Hydrothermal	UV-visible (Xe)	Ethanol	MoS_2/RGO	165.3	9.7 (365 nm)	>12 h	[72] (2012)
EY-MoS_2/RGO	N/A	Solution mixing	$\lambda \geq 420$ nm (Xe)	TEOA	MoS_2/RGO	83.8	24.2 (460 nm)	<6h	[73] (2012)
CdS/N-RGO	2	Solution mixing	$\lambda \geq 420$ nm (Xe)	Na_2S, Na_2SO_3	N-RGO	210	N/A	>30 h	[74] (2011)
Cu/P25/RGO	2	Hydrothermal	UV-visible (Hg)	Methanol	Cu/RGO	1275	N/A	<60 h	[75] (2012)
RGO	100	Hummers	UV-visible (Hg)	Methanol	None	2833	N/A	N/A	[40a] (2010)
Ni/RGO	97	Wet chemical	$\lambda \geq 420$ nm (Hg)	Methanol	Ni	~70	N/A	N/A	[76] (2012)
NiO/RGO	97	Wet chemical	$\lambda \geq 420$ nm (Hg)	Methanol	NiO	~30	N/A	N/A	[76] (2012)
$[Ru(bipy)_3]^{2+}$@ RGO	N/A	Solution mixing	$\lambda = 532$ nm (Laser)	Methanol	None	3290	N/A	<10 h	[77] (2012)
TiO_2/RGO	2	Hydrothermal	$\lambda \geq 420$ nm (Xe)	TEOA	Pt	380	8.2 (420 nm)	N/A	[78] (2012)

[a)]Xe, xenon lamp; TH, tungsten halogen lamp; Hg, high pressure Hg lamp; Laser, Nd/YAG laser. N/A: not available.

nanoparticles.[86,92] Transient photovoltage measurements also showed that the photovoltaic response of TiO_2/graphene composite was positive, and the mean life time of electron-hole pairs was prolonged from ~10^{-7} to ~10^{-5} s in comparison with that of TiO_2.[93] These findings directly proved that the photoinduced electrons could transfer from TiO_2 to RGO for preventing their combination with the holes. Thus, graphene as an electron acceptor/transporter can promote the separation of the photogenerated electron-hole pairs in TiO_2 semiconductor, transport the photogenerated electrons to reactive sites efficiently, and finally improve the photocatalytic H_2 production.[46] Furthermore, such a role of graphene has been found to be affected by several factors, including graphene content in the composite, interfacial interaction and contact area between graphene and TiO_2.

As an electron acceptor and transporter, graphene has been intensely investigated to achieve controllable photocatalytic H_2-production activities in the graphene/TiO_2 nanocomposite by varying graphene contents. For example, Cui group studied the photocatalytic performance of RGO/TiO_2 photocatalysts with weight ratio of RGO varying from 0 to 10%.[47] With increasing the content of RGO, the H_2-production rate of the sol-gel prepared RGO/TiO_2 composites increased to the highest value at 5% RGO. When the content of RGO was further increased, its photocatalytic activity decreased due to introduction of the electron-hole recombination centers into the composite.[47a] Similar results were obtained in the hydrothermal prepared RGO/TiO_2 photocatalysts by the same group.[47b] They believed that the enhanced photocatalytic property should be attributed to the electron acceptor and transporter role of RGO in the composite.

The electron acceptor and transporter role of graphene can also be significantly affected by the interfacial interaction between graphene and TiO_2. As the interfacial interaction is always related to the synthetic approach, such a role of graphene can be enhanced through rational design and synthesis of the graphene/TiO_2 composite. Fan et al.[48] prepared various P25/RGO photocatalysts by several techniques, including UV-assisted photocatalytic reduction, hydrazine reduction, and hydrothermal method. They found that the incorporation of RGO into P25 by any way could dramatically enhance the

Table 2. Graphene-based photoelectrodes for H_2 production by water splitting.

Photoelectrode	Preparation method	Incident light (source)	Electrolyte	Bias [V]	IPCE [%]	Ref. (year)
$BiVO_4$/RGO	Dropcasting	$\lambda \geq 420$ nm (Xe)	Na_2SO_4	0.75 (vs Ag/AgCl)	4.2 (400 nm)	[79] (2010)
ZnO/RGO	Electrophoresis	AM 1.5G (Xe)	Na_2SO_4	0.4 (vs Pt)	24 (400 nm)	[80] (2012)
α-Fe_2O_3/RGO/$BiV_{1-x}Mo_xO_4$	Spin-coating	AM 1.5G (Xe)	Na_2SO_4	–0.04 (vs Ag/AgCl)	0.53	[81] (2012)
Fe_2O_3/CNT-RGO	Spray coating	AM 1.5G (Xe)	NaOH	1.23 (vs Ag/AgCl)	~7 (400 nm)	[82] (2012)
α-Fe_2O_3/RGO	Electrodeposition	AM 1.5G (Xe)	NaOH	0.5 (vs Ag/AgCl)	~38 (400 nm)	[83] (2013)
Si/RGO	Spin-coating	UV-visible (Xe)	H_2SO_4,K_2SO_4	–0.754 (vs MSE)	N/A	[84] (2013)
TiO_2/RGO	Assembly	λ>420 nm (Xe)	Na_2SO_4	0 (vs Ag/AgCl)	0.0487[a)]	[85] (2012)

[a)] This value is the conversion efficiency of light energy to chemical energy.

Adv. Mater. **2013**,
DOI: 10.1002/adma.201301207

photocatalytic H_2 evolution; the stable P25/RGO prepared by the hydrothermal method showed the best performance and it could even catalyze the evolution of H_2 from pure water. It was proposed that an intimate contact was formed between P25 and RGO by the hydrothermal method, which accelerated the transfer of the photogenerated electrons from P25 to RGO by taking the advantage of the electron acceptor/transporter ability of graphene, thus enhancing the photocatalytic activity of the composite.

In addition to the interfacial interaction, the contact area between graphene and TiO_2 photocatalyst is another crucial factor that influences the electron acceptor/transporter role of graphene. Up to date, TiO_2/graphene composites with TiO_2 nanoparticles homogeneously distributed on graphene sheets have been prepared by various strategies, mainly including in situ growth, hydrothermal/solvothermal, solution mixing, and sol-gel method.[94] However, the 2D graphene sheets can only contact the bottom part of the TiO_2 nanoparticles in these composites, which limits the electron transport from TiO_2 nanoparticles to graphene. To solve this problem, a TiO_2@RGO core-shell photocatalyst for H_2 generation was designed by Choi group.[49] For synthesis of the core-shell photocatalysts, nanographene oxides (NGOs) were first prepared by a two-step chemical oxidation method and then self-assembled with TiO_2 nanoparticles to form a core-shell structure through dehydration condensation between the oxygen-containing functional groups on NGOs and the hydroxyl groups on the TiO_2 surface. The nanographene wrapped TiO_2 (r-NGOT) was finally ready by photocatalytic reduction of the NGO-coated TiO_2 in methanol solution under UV illumination (**Figure 2**a). The TiO_2 surface in r-NGOT was fully contacted by the RGO shell, resulting in the easier transfer of the photogenerated electrons from TiO_2 to RGO. On the other hand, Pt could be directly loaded on the core-shell composite due to the stronger synergetic interaction between Pt and r-NGOT, which shortened the transfer distance of electrons between Pt and r-NGOT. Thus, the H_2-production rate of r-NGOT was higher than that of RGO sheets loaded with TiO_2, as shown in Figure 2b.

However, it should be noticed that RGO used in most of the graphene/TiO_2 composites has much lower electrical conductivity than pristine graphene because of the existence of defects and functional groups, which limits the electron acceptor and transporter ability of graphene. To further improve the H_2-prodcution performance of the graphene-based material, high-quality graphene should be introduced to prepare the graphene/TiO_2 composites. There are already some attempts to synthesize graphene-based materials with less defective graphene to make full use of the unique electronic conductivity of graphene. One attempt is to use the solvent-exfoliated graphene (SEG) as graphene precursor. SEG is produced by utilizing ultrasonic energy to directly exfoliate graphite in suitable solvents, and possesses much lower defect density than RGO.[95] Several works have demonstrated the better photocatalytic performance of SEG/TiO_2 nanocomposites than that of RGO/TiO_2.[96] Thus the high-quality graphene can facilitate photocatalytic reactions by allowing photoinduced electrons to diffuse more effectively to reactive sites because of its improved electronic conductivity and a longer electronic mean free path.

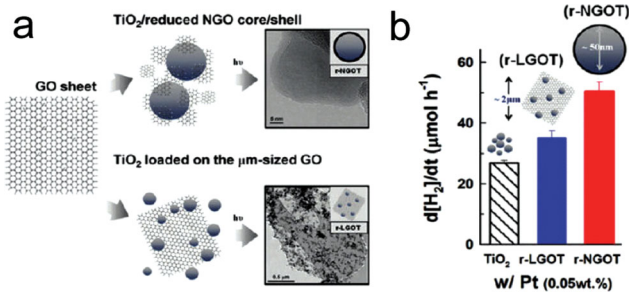

Figure 2. a) Illustration of the preparation procedure of r-NGOT and r-LGOT; b) Photocatalytic production of H_2 in the aqueous suspension of TiO2, r-LGOT, and r-NGOT in the presence of 0.05 wt% Pt ($\lambda > 320$ nm). Reprinted with permission.[49] Copyright 2011, American Chemical Society.

4.2. Graphene-Based Visible Light-Active System

As known to all, the UV region accounts for only ~4% of solar spectrum, while visible light occupies ~43% of the total irradiation energy of sunlight. Thus photoelectrodes/photocatalysts with excellent visible light response have been extensively investigated by introducing graphene as an electron acceptor and transporter, which can be divided into three main systems including graphene-semiconductor binary and trinary system, and dye-sensitized graphene-based system.

4.2.1. Graphene-Semiconductor Binary System

Among the various visible-light-driven photocatalysts, CdS is an attractive photocatalytic H_2-production material because of its narrow bandgap of 2.4 eV which can absorb an appreciable fraction of visible light. However, the photocatalytic activity of the CdS semiconductor is limited by the high recombination rate of the photoinduced electron-hole pairs. Cao et al.[97] reported a picosecond ultrafast electron transfer process from the photoexcited CdS to the graphene sheets in graphene/CdS nanocomposites using time-resolved florescence spectroscopy. This work demonstrated that graphene could act as an electron acceptor and transporter to reduce the recombination rate of the photoinduced electron-hole pairs in CdS photocatalysts. Also, Li et al.[43] investigated the photocatalytic H_2 generation property of the RGO/CdS nanocomposites prepared by a solvothermal method using $Cd(Ac)_2 \cdot 2H_2O$, DMSO, and GO as precursors, where the reduction of GO and the deposition of CdS on RGO were achieved simultaneously. As shown in **Figure 3**a, they found that the nanocomposites at the RGO content of 1.0 wt% and Pt 0.5 wt% reached a high H_2-production rate of 1.12 mmol h^{-1} under visible-light irradiation using lactic acid as a sacrificial reagent, corresponding an apparent quantum efficiency (AQE) of 22.5% at wavelength of 420 nm, which was enhanced by 4.84 times in comparison with that of the pure CdS/Pt. The enhancement of H_2-production rate was mainly attributed to the role of RGO as an electron acceptor and transporter to separate photogenerated electron-hole pairs (Figure 3b). Furthermore, excess RGO content also leaded to a deterioration of the photocatalytic performance similar to the graphene/TiO_2 system mentioned in Section 4.1, and it was attributed to the "shielding effect" which screened the reactive

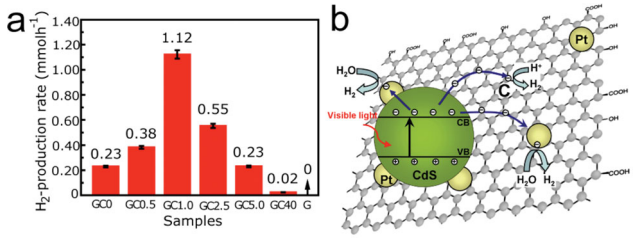

Figure 3. a) Comparison of the visible-light photocatalytic activity of samples GC0, GC0.5, GC1.0, GC2.5, GC5.0, GC40, and RGO for the H_2 production using 10 vol% lactic acid aqueous solution as a sacrificial reagent and 0.5 wt% Pt as a cocatalyst. b) Schematic illustration of the charge separation and transfer in the RGO/CdS system under visible light. Reprinted with permission.[43] Copyright 2011, American Chemical Society.

sites on the catalyst surface and decreased the light absorption of CdS in the RGO/CdS system. Later, Gao et al. and Peng et al. studied the visible-light-driven photocatalytic H_2-production activities of the RGO combined with CdS, and RGO as an electron acceptor and transporter improved the H_2-production activities in their systems.[51] Dong et al.[98] further investigated the interfacial electron-hole separation mechanism of the graphene-supported CdS nanomaterials using first-principles calculations. It was found that upon visible light irradiation the excited electron in CdS quantum dots (QDs) injected into graphene and transported along graphene layer through π^* orbitals to achieve interfacial electron-hole separation, which was in accordance with Li's experimental results.

Graphene was also used as the electron acceptor and transporter to combine with other visible light-active semiconductors to improve their H-$_2$-production activity. For example, Wang et al.[99] reported that the RGO/AgBr composite exhibited enhanced photocatalytic H_2 evolution as compared to bare AgBr nanosheets. Xiang et al.[56] demonstrated that the photocatalytic H_2-production rate of the RGO/g-C_3N_4 composite exceeded that of the pure g-C_3N_4 by more than 3.07 times owing to the efficient separation of the photogenerated electron-hole pairs and the lengthened lifetime of the charge carriers by incorporation of RGO. Yang et al.[53] presented a RGO/3C-SiC photocatalyst with a H_2-production rate of 95 μL h^{-1}, which was 1.3 times larger than that of the pure 3C-SiC nanoparticles. Lately, Mou et al.[57] prepared a novel $TiSi_2$/RGO composite using RuO_2 as a cocatalyst to produce H_2 from overall splitting of pure water under visible light irradiation. The resulting $RuO_2/TiSi_2$/RGO composite with 1 wt% RuO_2 and 1 wt% RGO showed a higher rate of H_2 evolution (64.2 μmol h^{-1} g^{-1}) than both of $RuO_2/TiSi_2$ composite (45.4 μmol h^{-1} g^{-1}) and pure $TiSi_2$ (37.3 μmol h^{-1} g^{-1}). In this system, the RGO sheets served as the electron acceptor, trapping the photogenerated electrons from $TiSi_2$ and/or RuO_2 particles and reducing the probability of electron-hole recombination. Simultaneously, O_2 was also evolved at high temperatures through the oxidation of water by holes in the VB of $TiSi_2$.

Doping of anions elements (N, S, C, etc.) into wide bandgap semiconductors (such as TiO_2) has been considered as an ordinary way to extend absorption to the visible light region, because the electrons can be excited directly from the heteroatom-formed impurity energy level to the CB under visible light irradiation. Unfortunately, the heteroatom-induced structural disorders and defects in these semiconductors can also function as recombination centers which limit their PEC/photocatalytic water splitting performance. On basis of the electron acceptor and transporter role of graphene, the recombination of the photoinduced electron-hole pairs might be partially suppressed in these doped semiconductors, thus increasing the water-splitting activity. For example, Pei et al.[50] prepared a visible-light-responsive nanocomposites consisting of N-doped TiO_2 with RGO. Its photocatalytic H_2-production efficiency was about 13.6 times higher than that of P25 photocatalyst. Mukherji et al.[55] synthesized RGO/$Sr_2Ta_2O_{7-x}N_x$ by photoinduced reduction of GO in the presence of N-doped $Sr_2Ta_2O_7$. By using RGO as an electron transfer highway to separate the charge carriers and as a support for the Pt cocatalyst, Pt-RGO/$Sr_2Ta_2O_{7-x}N_x$ photocatalysts showed higher average H_2-yield rate and quantum efficiency than both of the Pt/$Sr_2Ta_2O_7$ and Pt/$Sr_2Ta_2O_{7-x}N_x$ photocatalyst. Actually, graphene itself can also be used as a dopant for the wide bandgap photocatalyst to be active in the visible light region, which is analogous to the case of carbon-doped semiconductor.[47a,100] For example, Lee et al.[100c] reported a highly photoactive RGO-wrapped anatase TiO_2 nanoparticles with a significant reduced bandgap of 2.80 eV, in comparison with the bandgap of the bare anatase TiO_2 (3.2 eV). The TiO_2@RGO nanocomposites were synthesized through one-step hydrothermal treatment of the GO-wrapped amorphous TiO_2. During the hydrothermal treatment, the remaining unpaired π electrons of RGO could easily bond with more free Ti atoms on the surface of anatase TiO_2, resulting in the shift of the band edge similar to the effect of surface doping. Under visible light irradiation, strong photocurrent response was observed for the TiO_2/RGO nanocomposites, while no photocurrent was recorded for the bare anatase TiO_2 nanoparticles.

To further prove the role of graphene as an electron acceptor and transporter in the graphene-semiconductor binary system, time-resolved technique has been used. The time-resolved technique is a powerful experimental tool to investigate the dynamic properties of the photoinduced carriers in semiconductors, and has shown great potential for analyzing the photoinduced charge kinetics of graphene-based nanomaterials. For instance, time-resolved fluorescence spectroscopy has been extensively used for interface research on graphene-semiconductor nanocomposites such as graphene/CdSe,[101] graphene/CdS,[97] and graphene/CdTe.[102] Once combining graphene with the semiconductor, emission decay kinetics of the semiconductor nanocrystal decay much faster, and the photoluminescence (PL) lifetime of nanocomposites decreases with increasing graphene content, which is a direct proof of the electron transfer from the excited semiconductors to the graphene matrices. As a typical example, Kamat et al.[101] investigated the electron and energy transfer rates from photoexcited CdSe colloidal QDs to GO and RGO by analysis of excited state deactivation lifetimes as a function of degree of oxidation and charging in (R)GO. As shown in **Figure 4**a, with increasing GO concentration, the PL lifetime of CdSe decreased, and the contribution of the fast time decay component to the overall PL lifetime increased from 78.9% to 94.5%. This result confirmed the strong interactive nature

Adv. Mater. **2013**,
DOI: 10.1002/adma.201301207

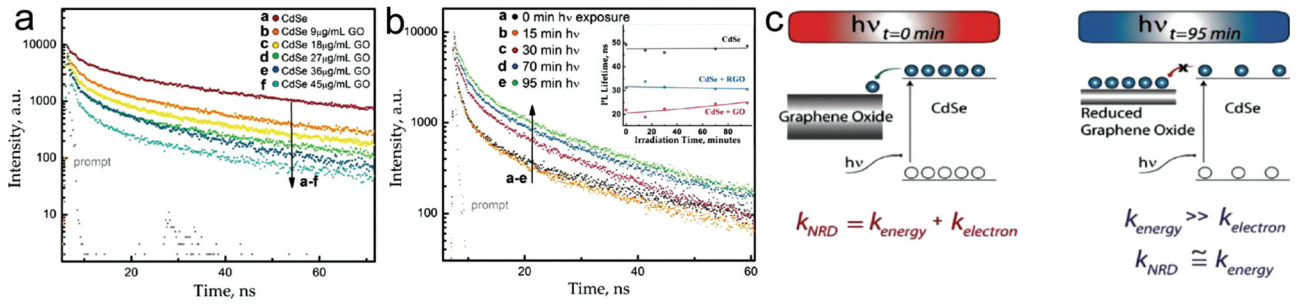

Figure 4. a) As the GO concentration increases, CdSe photoluminescence lifetimes become successively shorter. Excitation wavelength = 453 nm; long pass filter = 500 nm; fluorescence monitored at 508 nm. b) CdSe/GO composites show increased photoluminescence lifetimes upon visible light irradiation (>420 nm). Inset: The effect of visible light illumination (>420 nm) on CdSe photoluminescence lifetimes in the presence of GO and RGO is shown. c) Mechanism of energy and electron transfer from photoexcited CdSe colloidal quantum dots to GO and RGO. Reprinted with permission.[101] Copyright 2012, American Chemical Society.

between GO and CdSe QDs. With prolonged illumination by visible light, CdSe/GO composites showed increased PL lifetimes (Figure 4b), which was related to the different charging in GO. The mechanism illustrated in Figure 4c showed that initial illumination on CdSe/GO composite resulted in electron transfer from the CdSe CB to GO, while continued illumination resulted in a decrease in electron transfer rate because of the reduction of GO and eventual storage of electrons in GO. Thus PL decay was dominated solely by the energy transfer pathway with prolonged irradiation. Transient absorption spectroscopy and transient photovoltage technique were also executed to understand the charge transfer dynamics of graphene-semiconductor system including graphene/CdTe[102] and graphene/CdS[103] composites. The results demonstrated that the electron-holes were separated efficiently by transferring photoinduced electrons from semiconductors to graphene, and the recombination of electron-hole pairs in these excited semiconductor materials was retarded as well.

In addition to photocatalytic water splitting, PEC water splitting property of some visible light-active semiconductors have been investigated as well by using graphene as an electron acceptor and transporter. Ng et al.[79] firstly demonstrated that graphene could improve the H_2-production rate in the PEC cells. As shown in **Figure 5**, the working photoelectrode was fabricated by spin-coating technique using $BiVO_4$/RGO composites. A steady evolution of H_2 under visible light irradiation was quantified on the $BiVO_4$/RGO at a rate of 0.75 μmol h^{-1} with an external bias of 0.8 V, while negligible gas evolution was observed on pure $BiVO_4$. Moreover, the incident photon-to-current-conversion efficiency (IPCE) showed an enhancement to 4.2% for the $BiVO_4$/RGO in contrast to that of $BiVO_4$ (0.3% at 400 nm). The improvement was assigned to the usefulness of RGO in promoting charge collection and transport by accepting the photogenerated electrons from $BiVO_4$ and shuttling them to the collecting electrode, as well as the improved contact between the $BiVO_4$ particles and the transparent conducting electrode after using the RGO as scaffold. In another work, the PEC water splitting activity of silicon nanowires arrays was enhanced by spin-coating of RGO on top of these arrays, owing to the role of RGO as an electron acceptor and transporter which decreased the charge transfer resistance at the Si-electrolyte interface.[84] A graphene interlayer was also successfully

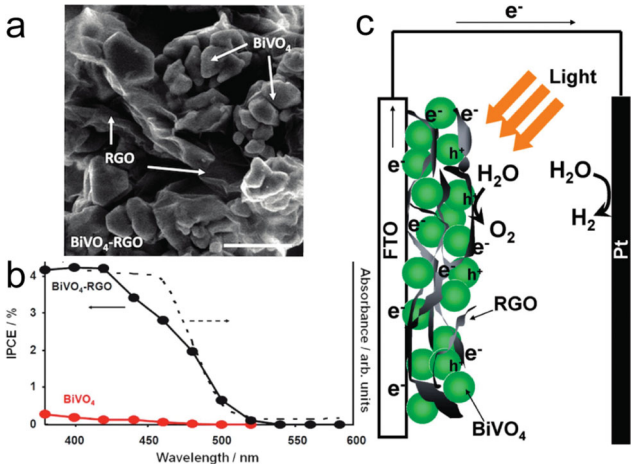

Figure 5. a) SEM image of $BiVO_4$-RGO samples. Scale bars correspond to 600 nm. b) IPCE and diffuse reflectance spectra of $BiVO_4$ and $BiVO_4$-RGO. c) Electron transport in a photoelectrochemical cell based on $BiVO_4$ and RGO. Reprinted with permission.[79] Copyright 2010, American Chemical Society.

inserted into inverse opaline hematite (α-Fe_2O_3) photoanodes for solar water splitting using the template assisted electrodeposition method.[83] The photocurrent density and IPCE of the RGO/α-Fe_2O_3 photoelectrode were remarkably improved compared to that of α-Fe_2O_3 photoelectrode. It was proposed that the graphene interlayer could act as both an electron transfer layer and an electrolyte blocking barrier, by which it not only reduced the charge recombination at the substrate-electrolyte interface but also helped the electron transportation from α-Fe_2O_3 to the substrate of the photoanode. Thus, graphene provides solutions to the fast charge recombination in the photoelectrode as well as the high charge transfer resistance at the photoelectrode-electrolyte interface in PEC cells.

The stability and long-term performance of photocatalysts is another primary concern for the practical applications. Some semiconductor photocatalysts such as CdS, ZnO, and Cu_2O suffer from photocorrosion through self-oxidization or self-reduction by photoinduced charges during the photocatalytic process, leading to degradation of the photocatalytic activity.[11a]

Combining semiconductors with graphene has the potential to avoid their photocorrosion, because the electron acceptor and transporter role of graphene is beneficial for extracting the photoinduced charges from semiconductors rapidly. For example, a recent study indicated that introducing RGO into the Cu_2O photocatalyst could dramatically improve the photostablility as well as the photocatalytic activity of Cu_2O.[67] In the experiment, there was a linear evolution of H_2 up to 15 hours before reaching a plateau using the Cu_2O/RGO photocatalyst; while the counterpart Cu_2O nanoparticles was completely deactivated after 5 hours due to the self-reduction of Cu_2O into Cu by the photoinduced electrons. Meanwhile, a photocurrent of 0.12 mA cm^{-2} and H_2 production of 1.4 μmol were obtained from the Cu_2O/RGO electrode at an applied bias of –0.4 V under visible light irradiation; while only 0.03 mA cm^{-2} photocurrent and 70 nmol H_2 were achieved from the pristine Cu_2O electrode. In this system, RGO acted as an electron acceptor to extract the photogenerated electrons from Cu_2O, suppressed the recombination of the photoinduced electron-hole pairs and prevented the self-reduction of Cu_2O into Cu, thus improving the photostablility of the composite.

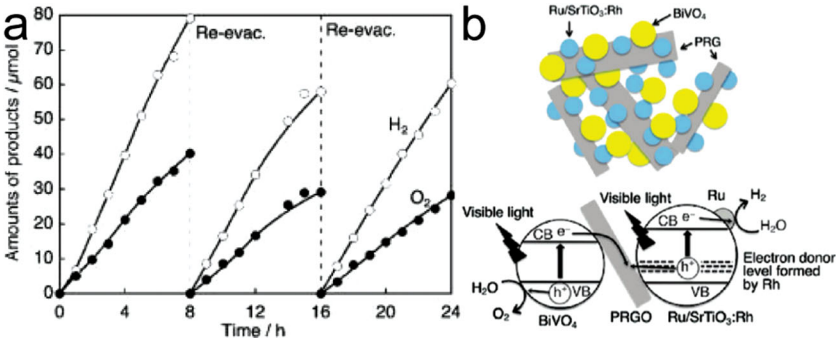

Figure 6. a) Overall water splitting under visible-light irradiation by the (Ru/$SrTiO_3$:Rh)-(RGO/$BiVO_4$) system; b) Schematic image of a suspension of Ru/$SrTiO_3$ and RGO/$BiVO_4$ in water at pH 3.5 (top) and mechanism of water splitting in a Z-scheme photocatalysis system consisting of Ru/$SrTiO_3$:Rh and RGO/$BiVO_4$ under visible-light irradiation (bottom). Reprinted with permission.[64] Copyright 2011, American Chemical Society.

4.2.2. Graphene-Semiconductor Trinary System

Besides previously mentioned binary systems, graphene as an electron acceptor and transporter has also attracted much attention in graphene-based trinary system for H_2 evolution recently. In this section, we will mainly introduce the use of graphene as an electron acceptor and transporter in Z-scheme and semiconductor heterojunction systems.

The biomimetic Z-scheme system, consisting of a H_2-evolution photocatalyst, an O_2-evolution photocatalyst, and an electron mediator, is an artificial photosynthetic system for overall water splitting into H_2 and O_2. Usually, the electron mediator is an ionic redox couple like IO^{3-}/I^- or Fe^{3+}/Fe^{2+}.[11b] Compared to the ionic redox couples, a solid mediator is more favorable in terms of reclamation of clean water and recovery of the photocatalyst. Considering the electron separation and transport ability, graphene could be a solid electron mediator, as demonstrated by Amal group.[64] They constructed series of Z-scheme systems using Ru/$SrTiO_3$:Rh, $BiVO_4$, and RGO (photoreduced GO). Among them, the Z-scheme system consisting of RGO/$BiVO_4$ and Ru/$SrTiO_3$:Rh showed the highest H_2-evolution rate, and RGO was stable as an electron mediator over a period of 24 hours (**Figure 6**a). Here RGO acted as an electron mediator, transferring the electrons from the CB of $BiVO_4$ to the impurity levels of Ru/$SrTiO_3$:Rh. The electrons in Ru/$SrTiO_3$:Rh reduced water to H_2 on the Ru cocatalyst, while the holes in $BiVO_4$ simultaneously oxidized water to O_2, accomplishing a complete water splitting cycle, as illustrated in Figure 6b. This work has paved a new way for design of new and efficient systems for H_2 production.

Constructing heterojunction nanostructures is a useful strategy to tackle the problem concerning low efficiency for H_2 evolution from solar water splitting, since the formed build-in electric field at the interface between different semiconductors can promote the separation and transport of photoinduced electron-hole pairs. There will be great potential for exploring the possibility of combining graphene with heterojunction nanostructures to help improve H_2 production using the electron acceptor and transporter function of graphene. For example, Hou et al.[66] synthesized CdS@TaON core-shell heterojunction coupled with RGO nanosheets. These photocatalysts showed a stable and high H_2-production rate of 633 μmol h^{-1} under visible-light irradiation at RGO content of 1 wt% and Pt content of 0.4 wt%, with an AQE of 31% at 420 nm, which was about 141 times higher than that of the pristine TaON. The high photocatalytic activity was ascribed firstly to the presence of CdS@TaON heterojunction that reduced the photogenerated electron-hole recombination; secondly to the involvement of RGO that served as an electron acceptor and transporter to efficiently lengthen the lifetime of the photogenerated charge carriers.

Graphene as an electron transporter between the two semiconductors of the heterojunction has also been applied successfully in PEC water splitting. Hou et al.[81] synthesized a novel heterojunction array of α-Fe_2O_3/RGO/$BiV_{1-x}Mo_xO_4$ core-shell nanorod with α-Fe_2O_3 as core, RGO interlayer, and $BiV_{1-x}Mo_xO_4$ shell, as shown in **Figure 7**a. The RGO interlayer was fabricated by photocatalytic reduction of GO, which was coated on Fe_2O_3 nanorod array (Fe_2O_3-NA) by a spin-coating method and follow-up nitrogen atmosphere annealing. As presented in Figure 7b, the α-Fe_2O_3/RGO/$BiV_{1-x}Mo_xO_4$ heterojunction exhibited a maximum photoconversion efficiency of ~0.53% at –0.04 V (0.56 V vs NHE), which were much higher than that of Fe_2O_3/RGO or Fe_2O_3. A possible water splitting mechanism was proposed in Figure 7c. When Fe_2O_3/RGO and $BiV_{1-x}Mo_xO_4$ formed a heterojunction, the difference between the Fermi levels of Fe_2O_3 and $BiV_{1-x}Mo_xO_4$ would lead to the shifts of their energy bands until their Fermi levels reached equilibrium. Upon irradiation, photogenerated holes and electrons appeared in the VB and CB of Fe_2O_3 and $BiV_{1-x}Mo_xO_4$, respectively. Thanks to the band alignment and potential difference, RGO sheets as an excellent electron conductor provided a direct pathway for electrons to transfer from the CB of $BiV_{1-x}Mo_xO_4$ shell to the CB of Fe_2O_3 core easily. The electrons in Fe_2O_3 then migrated to the

Adv. Mater. 2013,
DOI: 10.1002/adma.201301207

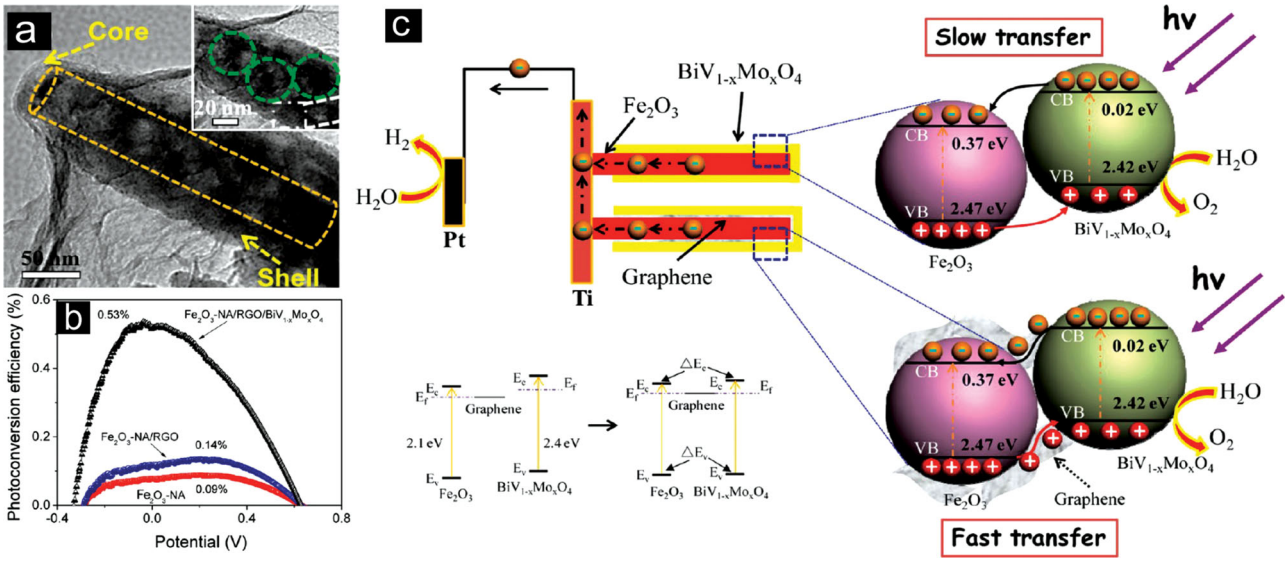

Figure 7. a) TEM image of Fe_2O_3-NA/RGO/$BiV_{1-x}Mo_xO_4$ heterojunction; b) photoconversion efficiency as a function of applied potential for Fe_2O_3-NA, Fe_2O_3-NA/RGO, and Fe_2O_3-NA/RGO/$BiV_{1-x}Mo_xO_4$ heterojunction in 0.01 M Na_2SO_4 solution under Xe lamp irradiation; c) Schematic for the energy band structure of the Fe_2O_3-NA/RGO/$BiV_{1-x}Mo_xO_4$ heterojunction and proposed mechanism of photoelectrochemical water splitting. Reprinted with permission.[81] Copyright 2012, American Chemical Society.

Ti substrate along the Fe_2O_3 nanorods, and ultimately transferred to the Pt electrode for H_2 evolution by reducing water under the external electrostatic field. Simultaneously, the holes in the VB of Fe_2O_3 which migrated to the VB of $BiV_{1-x}Mo_xO_4$ via the RGO interlayer would be consumed by oxidizing water to form O_2. Thus, the photoinduced charges were efficiently separated, resulting in the enhancement of PEC activity. This work opens a promising avenue for design and fabrication of novel graphene-based core-shell heterojunction for PEC water splitting.

4.2.3. Dye-Sensitized Graphene-Based System

Dye sensitization, another approach to broadening the solar light absorption, has been extensively used in the fields of solar cells[104] and semiconductor photocatalysis.[105] In principle, visible light excites the sensitizer molecules adsorbed on the photocatalyst, then the excited electrons subsequently inject to the CB of the photocatalyst. While the CB acts as a mediator for transferring electrons from the sensitizer to electron acceptors on surface of the photocatalyst, VB remains unaffected in a typical photosensitization.[106] However, the photo-to-energy conversion efficiency is always low owing to the poor electron transport between the dye and the photocatalyst. Considering the superior conductivity of graphene, using graphene as an electron acceptor and transporter between the photosensitizer and the catalysts provides an ideal way to design new dye-sensitized photocatalysts.

Based on the above speculation, Lu group reported an EY sensitized RGO with Pt nanoparticles dispersed on its surface for photocatalytic H_2 evolution under visible light for the first time.[58] The highest AQE of 9.3% was achieved under 520 nm irradiation using triethanolamine (TEOA) as a sacrificial reagent. In this case, RGO acted as an electron acceptor and transport mediate, transferring the electrons efficiently from EY photosensitizer to Pt, thus enhancing the photocatalytic H_2 evolution, as displayed in **Figure 8**a. Nevertheless, the rate of H_2 evolution linearly declined after 24 hours as a result of the partial degradation of EY. To address this issue, EY and Rose Bengal (RB) cosensitized RGO/Pt photocatalyst was constructed by the same group,[59] in which there was only a slight decrease in the photocatalytic activity after 40 hours irradiation. Since RGO could greatly facilitate electron transport from the photoexcited dyes to Pt, a high AQE up to 37.3% was obtained under 520 and 550 nm simultaneous light irradiation. More recently, they further systemically investigated the effects of the xanthenes dyes (EY, RB, fluorescein sodium, and rhodamine B), H_2 evolution catalysts (Pt, Pd, Rh, Ru, Au, Ag, and Ir), and sacrificial donors (TEOA, S^{2-}/SO_3^{2-}, H_2O, and EDTA) on the H_2-production rate of the dye-sensitized RGO systems.[60] Among them, RB sensitized RGO decorated with Pt nanoparticles using TEOA as the electron donor was proved to be the most active photocatalytic system for H_2 evolution, with an AQE of 18.5% at 550 nm, which was higher than those of RB-GO/Pt and RB-multiwall CNT/Pt photocatalysts under the same measured conditions. As discussed above, the graphene sheets acting as an electron acceptor and transporter can capture electrons from the excited dye due to its low-lying Fermi level, then transfer them to the decorated catalysts efficiently. Furthermore, graphene can afford large interfaces for well dispersing catalyst nanoparticles with more reactive sites, thereby enhancing the H_2-evolution efficiency.

Similarly, Mou et al.[61] reported the photocatalytic activities of an EY noncovalently functionalized RGO. The amount of H_2 production was 8.35 μmol for EY-RGO system under the UV-visible light irradiation for 2 hours, higher than those generated from RGO (4.86 μmol), GO (5.78 μmol), and EY-GO (6.09 μmol) systems. Zhu et al.[63] reported a $Ru(dcbpy)_3$ functionalized

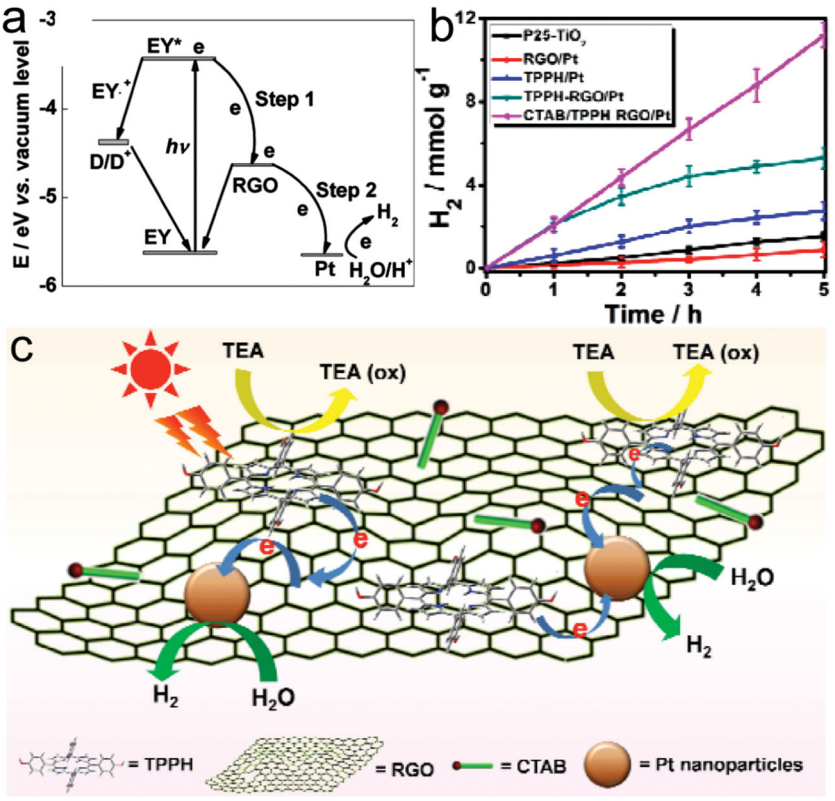

Figure 8. a) The energy level diagram for H_2 evolution over EY-RGO/Pt photocatalyst; Reprinted with permission. [58] Copyright 2011. American Chemical Society. b) The amount of H_2 evolved from as-prepared photocatalysts using TEA as a sacrificial agent under UV-visible light irradiation. Reaction conditions: $m_{catalyst}$ = 1 mg, RGO:TPPH = 2:1, [Pt] = 5 wt%, pH = 9, [TEA] = 10 vol%, [surfactant] = 2 mg, T = 298 K; c) Schematic photoexcited electron transfer and H_2 evolution over RGO-TPPH photocatalyst with the assistance of the CTAB under light irradiation. Reprinted with permission.[65] Copyright 2013, American Chemical Society.

RGO via the electrostatic and van der Waals interactions. The photocatalytic H_2 evolution amount of $Ru(dcbpy)_3$-RGO/Pt photocatalyst in TEOA aqueous solution was higher than those of RGO/Pt and $Ru(dcbpy)_3$/Pt. More recently, Zhu et al.[65] reported the photocatalytic H_2 generation of 5,10,15,20-tetrakis (4-(hydroxyl)phenyl) porphyrin (TPPH) non-covalently functionalized RGO nanocomposite (TPPH-RGO). As shown in Figure 8b, the TPPH-RGO/Pt nanocomposite exhibited remarkable enhanced photocatalytic H_2 production amount when compared with TPPH functionalized Pt colloid or Pt modified RGO, due to the superior electron-accepting and electron-transporting abilities of graphene. There was also a decrease after 2 hours of irradiation for the H_2-produciton activity of TPPH-RGO/Pt system, which was attributed to the aggregation of the TPPH-RGO nanocomposite during the photoreaction. To prevent the photocatalyst from aggregation, cetyltrimethylammonium bromide (CTAB) was used as a surfactant in the composite and the photocatalytic activity and stability of the TPPH-RGO/Pt photocatalyst was well improved. The tentative underlying mechanism for light-driven water reduction to produce H_2 on the TPPH-RGO/Pt nanohybrid with the assistance of CTAB is illustrated in Figure 8c. This investigation might shed light on the development of the stable dye-sensitized graphene photocatalysts with assistance of surfactants for H_2 generation.

In general, the functionalization of graphene sheets with dye molecules as photocatalysts can be performed by both noncovalent and covalent interactions. The former is of particular interest with respect to the protection of the electronic structure of graphene, since the driving forces for binding dye molecules and graphene is believed to be a combination of π–π^* electrostatic, π–π^* stacking, H_2 bonding or van der Waals interactions. The method of solution-mixing, i.e. the simple mixture of the dye molecules and the dispersed graphene suspension, is the most common noncovalent technique, and has been successfully used for graphene functionalized with many dye molecules, as discussed before. As for dye-covalently functionalized graphene photocatalyst, Li et al.[62] prepared a triphenylamine (TPA) functionalized RGO (G-TPA) via 1,3-dipolar cycloaddition, in which the TPA moiety covalently linked on the RGO nanosheets by an aziridino ring. The H_2-production rate and AQE of the Pt/G-TPA photocatalyst using KI as an electron donor was 2.3 μmol h^{-1} and 0.45% mol E^{-1}, respectively, under the irradiation of UV-visible light.

5. Graphene as a Cocatalyst

The cocatalyst is typically a noble metal or metal oxide or a combination of them, loaded on the surface of photocatalyst to enhance the charge separation, produce reactive sites, and reduce the activation energy for gas evolution. Usually, noble metals possess higher work function than those of semiconductors, so deposition of noble metal nanoparticles onto the surface of a semiconductor always makes electrons transfer from the CB of the excited semiconductor to metal and results in the formation of a schottky barrier, which can efficiently suppress the recombination of electrons and holes. Furthermore, most of metals have much lower overpotentials for H_2O reduction, indicating that they can provide plenty of reaction sites for absorbed protons. Therefore, noble metal cocatalysts have been widely applied for the enhancement of PEC/photocatalytic activities. However, noble metals are both costly and scarce, thus much attention has been focused on seeking novel low-cost cocatalysts recently. Graphene with a high work function has been widely accepted to behave like metals, and the reduction potential of graphene/graphene$^{\bullet-}$ is reported to be –0.08 eV, which is more negative than that of H^+/H_2.[44] Therefore, graphene is also a promising candidate for cost-effective cocatalyst to replace noble metals.

Zhang et al. constructed a noble metal-free RGO-$Zn_xCd_{1-x}S$ photocatalyst by a simple coprecipitation-hydrothermal strategy.[44] The optimized RGO-$Zn_{0.8}Cd_{0.2}S$ photocatalyst had a

Adv. Mater. 2013,
DOI: 10.1002/adma.201301207

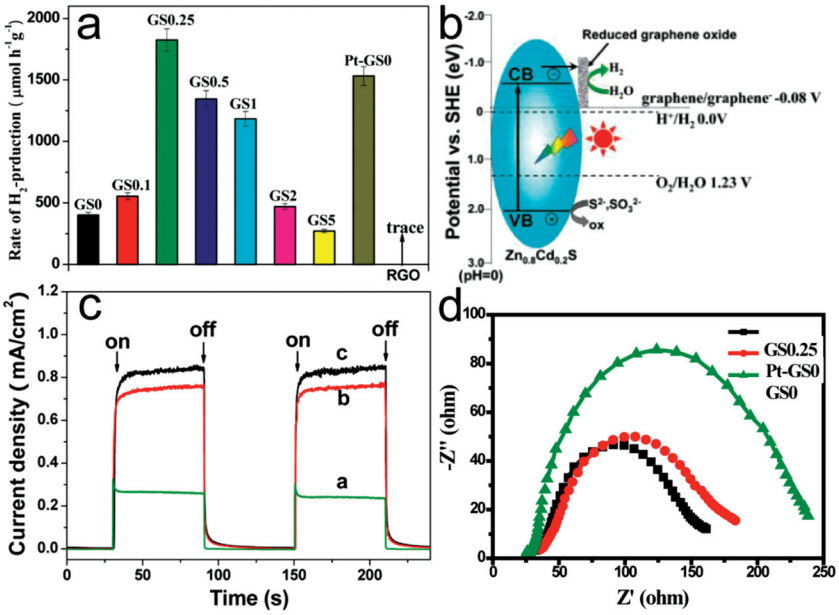

Figure 9. a) Comparison of the photocatalytic H_2-production activity under simulated solar irradiation over GS0, GS0.1, GS0.25, GS0.5, GS1, GS2, GS5, Pt-GS0 (1 wt% Pt), and RGO samples. b) Proposed mechanism for photocatalytic H_2-production under simulated solar irradiation. c) Transient photocurrent responses and d) Nyquist plots of $Zn_{0.8}Cd_{0.2}S$, 1 wt% Pt- $Zn_{0.8}Cd_{0.2}S$ and RGO/$Zn_{0.8}Cd_{0.2}S$ samples. Reprinted with permission.[44] Copyright 2012, American Chemical Society.

high H_2-production rate of 1824 μmol h^{-1} g^{-1} in Na_2S/Na_2SO_3 solution with an AQE of 23.4% at 420 nm, which was better than that of the optimized Pt-$Zn_{0.8}Cd_{0.2}S$ under the same reaction conditions (**Figure 9**a). The results suggested that RGO herein acted as a cocatalyst to extract photogenerated electrons from the CB of $Zn_{0.8}Cd_{0.2}S$ and promoted the charge separation, then reduced H^+ to H_2 molecule on its surface, as shown in Figure 9b. Besides, the space charge separation also prevented the reduction of Cd^{2+} and Zn^{2+} because of the close interaction between RGO and $Zn_{0.8}Cd_{0.2}S$. To further prove the above mechanism, Zhang et al. utilized electrochemical techniques including transient photocurrent response (TPC) and electrochemical impedance spectra (EIS), to investigate the charge-transfer properties at the graphene-semiconductor interface. Generally, TPC is recorded with several on-off cycles of intermittent irradiation, and can be normalized by the $I_{ph,in}/I_{ph,st}$ ratio, where $I_{ph,in}$ and $I_{ph,st}$ correspond to initial and stationary photocurrent, respectively.[107] The electrode with high $I_{ph,st}/I_{ph,in}$ ratio and $I_{ph,st}$ suggests a low recombination rate of electrons and holes in the photocatalyst materials. EIS can evaluate the charge transport and recombination properties within the photocatalyst films, which is presented in the form of Nyquist plots. The smaller arc diameter in Nyquist plots indicates a lower resistance of the interfacial charge transfer. As shown in Figure 9c and Figure 9d, the RGO-$Zn_{0.8}Cd_{0.2}S$ sample exhibited higher $I_{ph,st}$ in TPC and smaller arc diameter in EIS than Pt-$Zn_{0.8}Cd_{0.2}S$, indicating that the introduction of RGO could promote the separation of photoinduced charges and benefit the interfacial charge transfer. This finding reveals that graphene is a promising substitute for the noble metals in photocatalytic H_2-production.

The potential of RGO or graphene oxide as a cocatalyst in other photocatalytic systems was investigated as well. Yu group presented a RGO-modified TiO_2 composite with exposed {001} facets as a noble metal-free photocatalyst for H_2 evolution.[68] The highest H_2-production rate of the RGO/TiO_2 composite was 736 μmol h^{-1} g^{-1} even without Pt cocatalyst under UV-light illumination, which exceeded the rate observed on the pure TiO_2 by more than 41 times. Zhou et al.[54] reported a similar work by using the RGO/$ZnIn_2S_4$ nanosheet composite, which was fabricated via an "in situ controlled growth" solvothermal process. The obtained composite was demonstrated to be an excellent material for photocatalytic H_2-production with considerable stability, owing to the synergistic effect of its unique sheet-on-sheet structure. Lv et al.[69] investigated the photocatalytic H_2 evolution property of P25-RGO and CdS-sulfonated RGO, respectively. They found that CdS-sulfonated RGO had a better photocatalytic H_2 evolution rate than that of CdS-Pt, while photocatalytic H_2 evolution rate of P25-RGO was only 50% of that of P25-Pt. The work by Park et al.[70] showed the potential of RGO as an auxiliary cocatalyst to improve the photocatalytic H_2 generation rate of Pt/TiO_2. Besides, RGO was also found to be an efficient cocatalyst in CdS-metal oxide hybrids according to a recent work by Khan et al.[71] The AQY for H_2 evolution using CdS/ZnO/RGO, CdS/Al_2O_3/RGO and CdS nanoparticles was calculated to be around 30%, 14%, and 4%, respectively. All these findings confirm that RGO is an efficient cocatalyst to achieve highly efficient H_2 evolution.

Recently, graphene-based composites are also used as cocatalysts for photocatalytic H_2 generation. Xiang et al.[72] reported a trinary TiO_2/MoS_2/RGO photocatalyst (**Figure 10**a) prepared by a two-step hydrothermal process for H_2 evolution. Under UV-light irradiation, the TiO_2/MoS_2/RGO composite reached the highest H_2 production rate of 165.3 μmol h^{-1} with the layered MoS_2/RGO hybrid as a cocatalyst (Figure 10b), and the AQE reached 9.7% at 365 nm. As illustrated in Figure 10c, they proposed that the positive synergetic effect between MoS_2 and RGO sheets could suppress the charge recombination, improve the interfacial charge transfer, and provide a great number of active adsorption sites and photocatalytic reaction centers. Min et al.[73] further demonstrated that MoS_2/RGO hybrid could act as a high active cocatalyst for H_2 evolution in a dye sensitized photocatalytic system under visible light irradiation. A high AQE of 24.0% has been obtained at 460 nm over the EY-sensitized MoS_2/RGO photocatalyst. Another Cu/RGO cocatalyst was reported by Lv et al.,[75] and the H_2-generation efficiency from the Cu/RGO-P25 photocatalyst was about 5 times higher than that of the RGO-P25 photocatalyst due to the synergetic effect of Cu and RGO.

Heteroatom-doped graphene is also a good cocatalyst candidate for H_2 evolution reaction. For example, in a nitrogen-doped

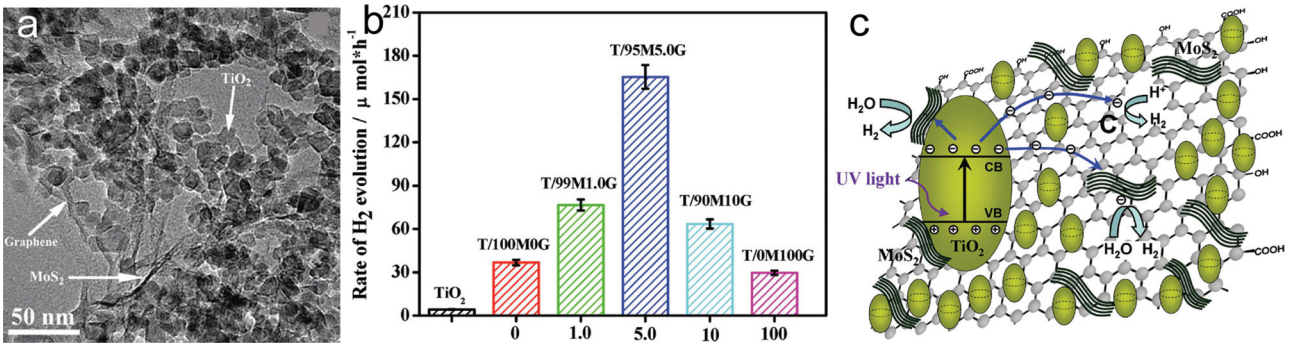

Figure 10. a) TEM images of T/95M5.0G composite. b) Photocatalytic H_2 evolution of TiO_2/MG composites with different MoS_2 and RGO contents in the MG hybrid as cocatalyst under UV irradiation. c) Schematic illustration of the charge transfer in TiO_2/MG composites. Reprinted with permission.[72] Copyright 2012, American Chemical Society.

graphene, the spin density and charge distribution of carbon atoms influenced by the neighboring nitrogen dopants will induce the "activation region" on the graphene surface, which can participate in catalytic reactions directly.[108] It has been reported that heteroatom-doped graphene is an efficient noble-metal free catalyst in oxygen reduction reactions and photodegradation of organic dyes.[109] Moreover, Jia et al.[74] synthesized a series of N-RGO/CdS nanocomposites in which N-RGO was obtained by annealing in NH_3 gas. And the highest H_2-production rate of 210 μmol h^{-1} was achieved under visible light irradiation, which was higher than those of the pure CdS (40 μmol h^{-1}) and GO/CdS. In addition, the cocatalyst of N-RGO as a protective layer could prevent CdS from photocorrosion under light irradiation.

6. Graphene as a Photocatalyst

Theoretical and experimental work[40a,110] has demonstrated that the CB minimum of RGO, which mainly formed by the anti-bonding π^* orbital, has a higher energy level (–0.52 eV vs NHE, pH = 0) than that needed for the H_2 generation, while the VB maximum of RGO is mainly composed of O 2p orbital that varies with the reduction degree (**Scheme 3**). As discussed in Section 3, the bandgap of RGO decreases with increasing reduction degree, suggesting that RGO with a suitable bandgap

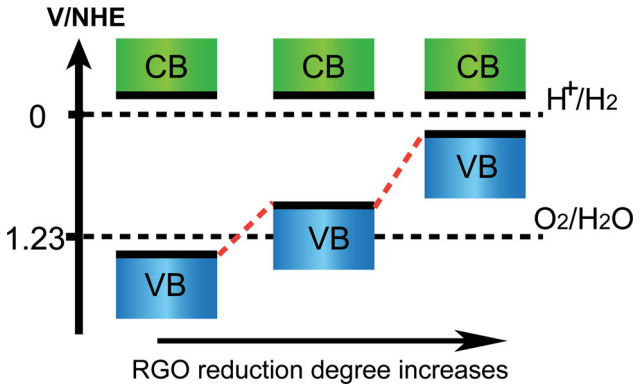

Scheme 3. Energy level diagrams of RGO with different reduction degree in comparison with the potentials for water reduction and oxidation.

for water splitting might be obtained by tuning its reduction level.[8,38c]

Yeh et al.[40a] proved the photocatalytic H_2-evolution activity of RGO for the first time using the RGO sample with the bandgap of 2.4–4.3 eV. As shown in **Figure 11**a, RGO exhibited stable H_2 evolution from an aqueous methanol solution or pure water, even without Pt cocatalyst under mercury light irradiation. They also investigated the photocatalytic activity of RGO with various oxidation levels.[111] The results showed an inverse relationship between the amount of H_2 evolution and the population of the oxygen-containing groups on the RGO sheets. They concluded that the RGO with higher oxidation degree had a larger bandgap and limited absorption of light, thus exhibiting a lower photocatalytic activity than the RGO with lower oxidation degree (Figure 11b). It was also found that the H_2-evolution rate was stable over time, whereas the O_2 evolution exhibited a decreasing trend. This could be explained that the electronic structure of the RGO with a sufficient oxidation degree was suitable for both the reduction and oxidation of water under illumination. However, the mutual reduction between the RGO sheets narrowed their bandgaps during the photocatalytic reaction, leading to the upward shift of the VB edge, whereas the CB edge remained almost unchanged (Figure 11c). Matsumoto et al.[112] also reported the photoreactions to generate H_2 from an aqueous suspension of RGO nanosheets or a RGO/ITO photoelectrode under UV irradiation. The findings demonstrate that RGO with an appropriate reduction level can serve as a photocatalyst for H_2 evolution.

Agegnehu et al.[76] deposited Ni and NiO cocatalysts on the prepared RGO sheets to enhance the photocatalytic activity of RGO. The H_2 evolution rate of NiO/RGO and Ni/RGO from aqueous methanol solution under UV-visible light illumination was enhanced by approximately 4- and 7-fold compared to that of the bare RGO, respectively. In comparison with Ni/RGO, the relatively lower activity of NiO/RGO was attributed to the less efficient electron trapping ability of the NiO surface, which caused more electrons recombination with holes.

Recently, Latorre-Sánchez et al.[77] reported that the photocatalytic activity of RGO for H_2 generation from water and methanol mixtures under visible light could be improved by the presence of dyes. The most efficient photocatalyst was a few layers of $[Ru(bipy)_3]^{2+}$ incorporated RGO with a moderate degree of

DOI: 10.1002/adma.201301207

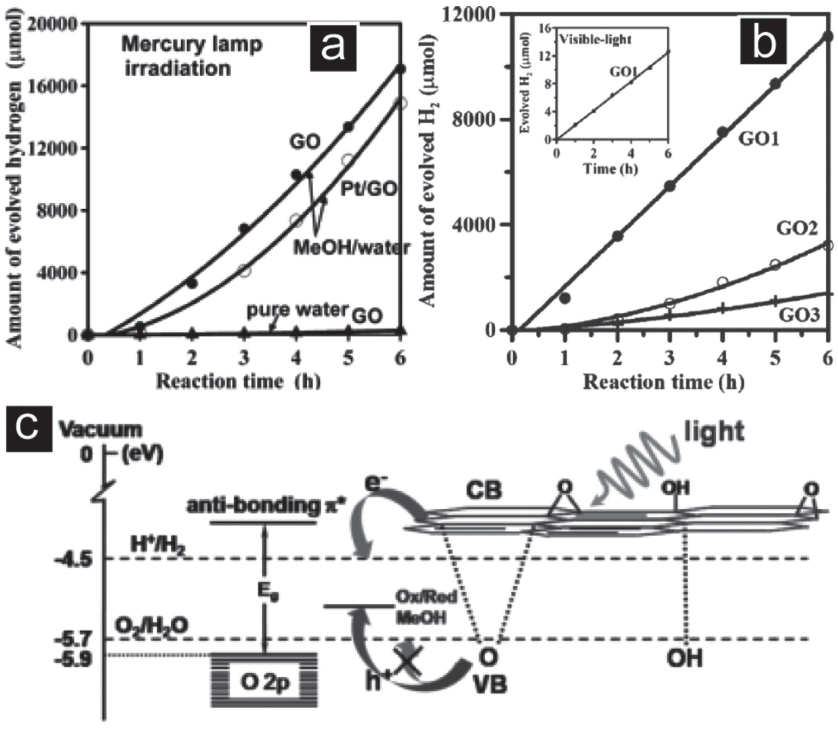

Figure 11. a) Time course of H_2 evolution from a 20 vol% aqueous methanol solution (MeOH/water) or pure water with suspended photocatalysts (RGO or Pt/RGO) (0.5 g) under mercury-lamp irradiation.[40a] b) Time course of H_2 evolution from a 20 vol% aqueous methanol solution suspended with 0.5 g of RGO photocatalysts with different oxidation levels (GO1 < GO2 < GO3) under mercury-lamp irradiation; Reprinted with permission from ref. [106]. Copyright 2011, American Chemical Society. c) Schematic energy-level diagram of RGO relative to the levels for H_2 and O_2 generation from water. Reproduced with permission.[40a]

oxidation (GO1), as shown in **Figure 12**a. The AQY for H_2 evolution was 0.12% for the optimized $[Ru(bipy)_3]^{2+}$@GO1 at 532 nm, which was higher than that of GO1 (0.008%). The proposed mechanism for electron transport was illustrated in Figure 12b. Due to strong interfacial interaction and orbital overlapping between GO1 and the dye molecular, the electrons in LUMO of $[Ru(bipy)_3]^{2+}$ were injected into the CB of GO1 firstly upon light irradiation, then consumed by the absorbed protons, resulting in the formation of H_2. However, there was a decrease in photocatalytic activity due to the decomposition of the dye and the changes in RGO structure (Figure 12c). Nevertheless, this work opens up new opportunities for the design of graphene derivative photocatalysts with enhanced photocatalytic H_2-production performance.

7. Graphene as a Photosensitizer

Graphene has been widely considered to accept electrons from photoexcited semiconductors as discussed above. However, the transfer of photoexcited electrons from graphene to semiconductor has also been observed according to several experimental and theoretical researches. Very recently, a visible-light-response ZnS/RGO photocatalysts were reported, and RGO in the nanocomposites was proved to act as an organic dye-like macromolecular "photosensitizer" instead of an electron reservoir for ZnS.[113] Similarly, other graphene-based wide bandgap semiconductors, such as TiO_2/RGO and $ZnWO_4$/RGO, also exhibited excellent photocatalytic activity in dye degradation under visible light irradiation owing to the photosensitization of graphene.[114] In these work, the photosensitizer role of graphene was explained as following: the electrons on the HUMO of graphene were firstly excited to the LUMO of graphene under visible light irradiation, then the photoinduced electrons in graphene were injected to the CB of semiconductor followed by taking part in the reduction reaction on the surface of semiconductor, thus producing the visible light activity. Amal and co-workers[115] studied the interfacial charge transfer of graphene/titania hybrid by ab initio calculations. It was interesting that electrons could be directly excited from the upper VB of graphene to the CB of titania under visible light irradiation. Du et al.[116] explored the interfacial charge transfer between g-C_3N_4 and graphene. They found that the inhomogeneous planar g-C_3N_4 substrate could form a well-defined electron-hole puddle on the supported graphene layer, driving the

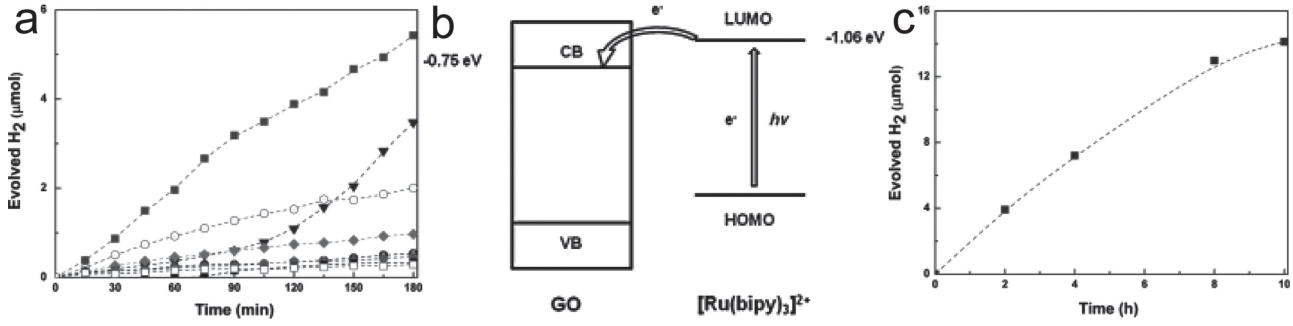

Figure 12. a) Amount of H_2 evolved during photocatalysis with GO1 and a series of dyes as the photocatalyst and methanol as the sacrificial under $\lambda = 532$ nm laser irradiation. b) Schematic diagram showing the electron injection from the LUMO of $[Ru(bipy)_3]^{2+}$ to the CB of GO1 (V vs. Ag/AgCl). c) Amount of H_2 evolved during a photocatalytic run with $[Ru(bipy)_3]^{2+}$@GO1 (0.02 g L^{-1}) as the photocatalyst and methanol as the sacrificial electron donor under $\lambda = 532$ nm laser irradiation for 10 h. Reproduced with permission.[79]

interlayer charge transfer from the VB of graphene to the CB of g-C_3N_4. These results directly proved that the photoinduced electrons in graphene could be successfully transferred to the CBs of semiconductors. Thus the above findings clearly demonstrate another potential role of graphene — photosensitization in some semiconductor-graphene hybrids.

The role of graphene as a photosensitizer has also been reported in light-driven water splitting by several related work. For example, Zeng et al.[78] reported a RGO/TiO_2 nanocomposite prepared by a facile hydrothermal method. The obtained RGO/TiO_2 had an optimal photocatalytic H_2-production rate of 380 μmol h^{-1} under visible light irradiation, giving an AQE of *ca*. 8.2% at 420 nm. The mechanism was described as follows: upon visible light irradiation, the excited photo-generated electrons from RGO photosensitizer were subsequently injected into the CB of TiO_2 due to the d-π interaction, then the excited electrons were transferred to the active sites on TiO_2 to produce H_2. Song et al.[85] also demonstrated the sensitizing effect of RGO on TiO_2 nanotube arrays. A maximum photoconversion efficiency of 0.0487% was obtained for the RGO modified TiO_2 photoelectrode under visible light, which was enhanced by 15 times compared to that of the pristine TiO_2.

Lin et al.[80] hybridized the ZnO nanorod array with graphene by the electrophoresis technique, and investigated its PEC properties. They found that the RGO-ZnO heterojunction displayed substantial photoactivity in the visible-light region from 400 to 450 nm in addition to the strong photoresponse in the near-UV region, and the IPCE at 400 nm was up to 24%. Furthermore, the rate of H_2 evolution of the Pt-RGO-ZnO photoelectrode was 5 times of magnitude higher than that of the bare ZnO at a bias of 1 V under UV-visible light irradiation. They concluded that RGO acted as a photosensitizer in the RGO-ZnO hybrid, improving the light response of ZnO, thus promoting the H_2 evolution reaction.

8. Graphene vs Other Carbon Nanomaterials

The extended honeycomb network of graphene is the basic building block of other important allotropes of carbon. 2D graphene can be wrapped to form 0D fullerenes, rolled to form 1D carbon nanotubes (CNT), and stacked to form 3D graphite. Before the discovery of graphene, fullerene, CNT and graphite have already been recognized as useful materials in light-driven water splitting systems.[117] Particularly, CNT is extensively applied to improve the energy conversion efficiency in solar energy conversion field, owing to its outstanding structural and electrical properties. Similar to graphene, CNT has also been reported to serve as an electron acceptor/transporter,[118] a cocatalyst,[117e] and a photosensitizer[117f] in solar water splitting. Therefore, the comparison between graphene- and CNT-semiconductors as photocatalysts/photoelectrodes is constantly mentioned and discussed, which is necessary and inevitable, for a complete understanding on the unique contribution of graphene for the enhancement of the H_2-production performance.

In general, graphene has some advantages over CNT in the application for PEC/photocatalytic H_2 evolution. First, graphene possesses an ultrahigh theoretical specific surface area of 2630 m^2 g^{-1} and optical transparency of 97.7%, which are both higher than those of CNT (1315 m^2 g^{-1} for specific surface area[119] and 95.7% for optical transparency[120]). This makes graphene more desirable to provide sufficient reactive sites for H_2 generation than CNT. Especially in the tandem PEC cells, the increase of surface area promotes charge transfer across the material interfaces (solid-solid and solid-liquid), allowing the better match of the photocurrents with the slow kinetics of the water redox reactions and reducing the need for highly active and often expensive cocatalysts. Second, the contact area or interfacial interaction between semiconductors and graphene is commonly larger than that between semiconductors and CNT even using the same preparation strategy, because CNT is a tubular structure with a curvature. The sheet-structured graphene also has better ability to disperse other nanomaterials for obtaining larger overall specific surface area compared to CNT with a tube-structure. Third, graphene has higher conductivity and mobility than CNT, since the degree of curvature presented by the extended π-aromatic structure in graphene is lower than that in CNT. For example, the room-temperature mobility of electrons is 200000 cm^2 V^{-1} s^{-1} for pristine graphene, which is almost three times higher than that for CNT (79000 cm^2 V^{-1} s^{-1}).[121] Thus, theoretically graphene should be better than CNT for use in solar hydrogen generation regarding to its larger specific surface area, better contact with semiconductor, and higher electrical conductivity than CNT. For example, Ye et al.[122] reported that the CdS/RGO composite was more efficient than the CdS/CNT composite in photocatalytic H_2 generation under visible light irradiation due to the better contact between CdS and RGO. In addition, graphene is nontoxic and biocompatible;[123] while CNT was reported to be cytotoxic in many papers.[124] So, graphene might be more suitable for future large-scale production without detrimental effect on environment compared to CNT. Otherwise, functionalized graphene or graphene oxide itself is a photoactive material for H_2 generation as discussed in Section 6. Whereas, CNT has not yet been reported as a photocatalyst for H_2 generation to the best of our knowledge.

Among the merits for water splitting, Kim et al.[125] suggested that the electrical conductivity of carbon materials should be a primary physicochemical property in determining the H_2 production, other than the surface area or other factors. In their experiment, CNT/CdSe photocatalyst showed higher H_2-production activity than RGO/CdSe photocatalysts because CNT had a better electrical conductivity than RGO. However, RGO/CdSe could show better photocatalytic activity than CNT/CdSe if the electrical conductivity of RGO was optimized, since it was reported that the electrical conductivity of RGO was approximately 60 times better than that of CNT.[126] And Xu et al.[127] stated that graphene-based nanomaterials was in essence the same as other carbon composite nanomaterials on enhancement of photocatalytic activity. In fact, PEC/photocatalytic H_2-generation reaction involves many factors such as the physicochemical property of semiconductors and the interaction between semiconductor and carbon materials, and the result is usually attributed to the synergistic effect among all these factors. So, it is hard to clarify whether the graphene-based material is wholly superior to other carbon-based material for use in H_2 generation, even for comparison in one aspect it must be sure that all other factors influencing the performance

Adv. Mater. **2013**,
DOI: 10.1002/adma.201301207

are strictly identical in the contrast test. And as commend by Dou,[128] it was too early to get a decisive answer for graphene's superiority over other carbon materials.

In other ways, a few downsides might limit the solar water splitting activity of graphene- or CNT-based nanomaterials. For instance, the contact area between graphene or CNT and semiconductor nanoparticles is always confined, as the 2D graphene scaffold usually contacts the bottom part of the nanoparticles, and the CNT scaffold self-entangles easily; the conducting property of graphene or CNT also gets deteriorated due to their functionalized surface, defects or disorders. Kim et al.[129] found that 3D conducting composite of graphene-CNT/Fe_2O_3 exhibited an enhanced PEC water splitting activity exceeding by 270 and 220% compared to graphene/Fe_2O_3 and CNT/Fe_2O_3, respectively. It was because graphene could act as a spacer role to separate CNTs, suppressing the self-agglomeration of CNT, and vice versa. As a result, the contact area between graphene or CNT and semiconductors could be enlarged. Furthermore, graphene could behave as additional electron transport pathways between CNTs, while CNT could serve as conducting channels between graphene sheets. Therefore, the graphene-CNT/Fe_2O_3 composite showed better water splitting performance than the graphene/Fe_2O_3 and CNT/Fe_2O_3. Obviously, the synergistic effect of these two carbon materials on improving the structural and conducting properties will attract some attention for solar water splitting.

9. Concluding Remarks

Graphene has been widely applied in H_2 generation from light-driven water splitting as a new type of carbon nanomaterial. And it not only shows the ability in separating the photogenerated electrons-hole pairs, superseding noble metals, increasing photostablility, and broadening light absorption, but also exhibits the capacity for photocatalytic H_2 evolution by itself. Nevertheless, research on the graphene-based materials for H_2 generation from light-driven water splitting is still at the initial stage, and there are many challenges for significantly improving PEC/photocatalytic performance or possibly leading to breakthrough. Some issues are listed as follows:

(1) Synthesis of graphene-based materials. The PEC/photocatalytic activity of graphene-based materials is highly dependent on their physicochemical properties, such as composition and morphology. Most of graphene-related materials for water splitting are prepared following a chemical route from GO in the shape of sheet. Substantially enhancing the H_2 generation efficiency of graphene-based materials can be expected by tuning the composition and optimizing the morphology. Therefore, extra efforts have to be made for rational design and synthesis of graphene-based photoelectrodes or photocatalysts so that the properties and functions of graphene can be fully utilized. Take graphene grown by chemical vapor deposition (CVD) as an example, the conductivity is much better than that synthesized by chemical reduction of GO and the scalability is more suitable for large-size photoelectrode; single- and multiple-doping of heteroatom in graphene can tune its many properties. Furthermore, the doped graphene can give rise to multiple exciton generation (MEG), i.e. formation of several electron-hole pairs after absorption of one photon.[130] This MEG effect will extremely enhance the hydrogen production efficiency if applied to solar water splitting. In addition, graphene with different dimensionality ranging from 0D graphene quantum dots (GQDs), 1D graphene nanoribbons, 2D graphene sheets, to 3D porous frameworks, has special electronic and optical properties.[131] For instance, GQDs have light response ranging from UV through visible into infrared depending on their specific size, geometry, and boundary conditions. More importantly, GQDs have remarkable upconversion ability to convert low-energy photons into high-energy photons and exceptionally long lifetime of hot carriers,[132] which have been successfully applied to improve the photovoltage or photodegradation activity of semiconductors as the electron-acceptor or photoabsorber.[133] The unique properties of GQDs might be beneficial to separation of photoinduced charges and absorption of light in solar water splitting. Therefore, design and synthesis of graphene with desired composition, size, edge structure, and dimensionality is worthy of exploration for enormously improving the performance of the PEC/photocatalytic H_2 evolution.

(2) Comprehensive roles of graphene. A few roles of graphene in H_2 production from water splitting were discussed in this review, while it is far from completed. It is reported that the strong synergetic interaction between graphene and semiconductor improves the charge separation and transfer properties in the photoexcited semiconductor and affects the band structure of graphene. The coupling interaction usually opens up a bandgap in the zero-bandgap graphene and induces doping effect in the carbon monolayer. However, the semiconducting properties of graphene in the composite are usually ignored when graphene is used as the electron acceptor and transporter, even with RGO as the building block. Besides, the defects in carbon nanomaterials are of importance for their electronic properties, and play a critical role in enhancement of the electrochemical stability and catalytic activity of the supported catalysts.[134] Thus, the structure defects of graphene should be paid much attention to in the future work, which might be the active sites for H_2 evolution. Otherwise, the photosensitization of graphene in H_2 generation is lack of direct experimental support in spite of enough evidence in support of graphene as an electron acceptor. For semiconductor/RGO hybrids, the photosensitization may also come from the isolated semiconducting sp^2 clusters of aromatic rings within the matrices of RGO in addition to the reported mechanism as discussed in Section 7.[135] So, the functions of graphene in photocatalytic reactions need to be better studied for a thorough and clear picture of the underlying mechanism.

(3) Theoretical calculation of graphene-based materials. Numerous experimental results have already demonstrated the crucial roles of graphene in the enhancement of solar conversion efficiency. However, the inherent mechanism behind the enhancement of H_2-production activity is still not well clarified for graphene-based materials at the present stage, since the current experimental technologies cannot provide direct evidence for the strengthened interfacial charge transfer property. Whereas theoretical calculation can almost perfectly simulate all these specific microstructures, and provide

in-depth insight to the electronic properties of nanomaterials, giving us a better understanding of the experimental phenomena.[136] Therefore, theoretical calculation has been considered as one of the most powerful means to investigate the photoinduced charge transfer between graphene and semiconductor at the molecular level, which is pivotal for revealing the underlying photocatalytic mechanism of the composite semiconductors. Furthermore, considering the various morphologies of graphene and the diverse choice of photoactive materials, it is incredible to try out all the possible combinations for H_2 generation from solar water splitting experimentally. Theoretical calculation has been demonstrated to be capable of simulating catalytic reactions at surfaces with the detail and accuracy required for computational results which compare favourably with experiments. Hence, theoretical calculation holds great potential for screening for catalysts with increased activity, designing new photocatalysts, and engineering the electronic structures of the active surface by changing the composition and structure of the graphene-based composites besides describing the photocatalytic reactions.

Study targeting efficient hydrogen generation from solar water splitting by graphene-based materials is inherently interdisciplinary, involving chemistry, physics, materials, and engineering. It is a very exciting research avenue, and challenges as well as opportunities coexist. The intense and rational efforts and close cooperation among researchers in different fields would make a great breakthrough for hydrogen energy development by utilizing graphene-based materials, which we believe will be far beyond what has been reported in this review paper and be beneficial for human being on both economic and environmental aspects.

Acknowledgements

The authors acknowledge partial financial support for this work from the National Natural Science Foundation of China (Nos. 91123003, 21005023), the National Basic Research Program of China (No. 2011CB933401), and the Knowledge Innovation Program of the Chinese Academy of Sciences.

Received: March 15, 2013
Published online:

[1] N. S. Lewis, *Science* **2007**, *315*, 798.
[2] J. A. Turner, *Science* **1999**, *285*, 687.
[3] O. Akhavan, *ACS Nano* **2010**, *4*, 4174.
[4] P. Millet, F. Andolfatto, R. Durand, *Int. J. Hydrogen Energy* **1996**, *21*, 87.
[5] W. Kreuter, H. Hofmann, *Int. J. Hydrogen Energy* **1998**, *23*, 661.
[6] T. Pregger, D. Graf, W. Krewitt, C. Sattler, M. Roeb, S. Möller, *Int. J. Hydrogen Energy* **2009**, *34*, 4256.
[7] M. Ni, D. Y. C. Leung, M. K. H. Leung, K. Sumathy, *Fuel Process. Technol.* **2006**, *87*, 461.
[8] M. G. Walter, E. L. Warren, J. R. McKone, S. W. Boettcher, Q. Mi, E. A. Santori, N. S. Lewis, *Chem. Rev.* **2010**, *110*, 6446.
[9] A. Fujishima, K. Honda, *Nature* **1972**, *238*, 37.
[10] A. J. Bard, *J. Photochem.* **1979**, *10*, 59.
[11] a) A. Kudo, Y. Miseki, *Chem. Soc. Rev.* **2009**, *38*, 253; b) X. Chen, S. Shen, L. Guo, S. S. Mao, *Chem. Rev.* **2010**, *110*, 6503; c) K. Maeda, K. Domen, *J. Phys. Chem. Lett.* **2010**, *1*, 2655; d) M. A. Fox, M. T. Dulay, *Chem. Rev.* **1993**, *93*, 341; e) A. Fujishima, X. Zhang, D. A. Tryk, *Int. J. Hydrogen Energy* **2007**, *32*, 2664; f) P. V. Kamat, *J. Phys. Chem. C* **2007**, *111*, 2834; g) A. J. Esswein, D. G. Nocera, *Chem. Rev.* **2007**, *107*, 4022; h) H. Tong, S. Ouyang, Y. Bi, N. Umezawa, M. Oshikiri, J. Ye, *Adv. Mater.* **2012**, *24*, 229; i) X. Chen, S. S. Mao, *Chem. Rev.* **2007**, *107*, 2891; j) A. L. Linsebigler, G. Lu, J. T. Yates, *Chem. Rev.* **1995**, *95*, 735; k) F. E. Osterloh, *Chem. Mater.* **2007**, *20*, 35.
[12] a) C. J. Li, G. R. Xu, B. Zhang, J. R. Gong, *Appl. Catal. B* **2012**, *115–116*, 201; b) C. J. Li, J. N. Wang, B. Wang, J. R. Gong, Z. Lin, *Mater. Res. Bull.* **2012**, *47*, 333; c) C. J. Li, J. N. Wang, B. Wang, J. R. Gong, Z. Lin, *J. Nanosci. Nanotechnol.* **2012**, *12*, 2496; d) K. Zhang, Q. Liu, H. Wang, R. B. Zhang, C. H. Wu, J. R. Gong, *Small* **2013**, 10.1002/small.201300841.
[13] a) K. Domen, A. Kudo, T. Onishi, *J. Catal.* **1986**, *102*, 92; b) K. Domen, S. Naito, T. Onishi, K. Tamaru, *Chem. Phys. Lett.* **1982**, *92*, 433.
[14] a) H. Kato, A. Kudo, *Catal. Lett.* **1999**, *58*, 153; b) A. Kudo, H. Kato, *Chem. Phys. Lett.* **2000**, *331*, 373.
[15] a) K. Maeda, K. Teramura, N. Saito, Y. Inoue, H. Kobayashi, K. Domen, *Pure Appl. Chem.* **2006**, *78*, 2267; b) G. Hitoki, A. Ishikawa, T. Takata, J. N. Kondo, M. Hara, K. Domen, *Chem. Lett.* **2002**, *7*, 736; c) A. Ishikawa, T. Takata, T. Matsumura, J. N. Kondo, M. Hara, H. Kobayashi, K. Domen, *J. Phys. Chem. B* **2004**, *108*, 2637; d) A. Ishikawa, T. Takata, J. N. Kondo, M. Hara, H. Kobayashi, K. Domen, *J. Am. Chem. Soc.* **2002**, *124*, 13547; e) G. Hitoki, T. Takata, J. N. Kondo, M. Hara, H. Kobayashi, K. Domen, *Chem. Commun.* **2002**, *16*, 1698.
[16] a) M. Yashima, H. Yamada, K. Maeda, K. Domen, *Chem. Commun.* **2010**, *46*, 2379; b) K. Maeda, K. Teramura, D. Lu, T. Takata, N. Saito, Y. Inoue, K. Domen, *Nature* **2006**, *440*, 295; c) K. Maeda, K. Teramura, D. Lu, N. Saito, Y. Inoue, K. Domen, *J. Phys. Chem. C* **2007**, *111*, 7554; d) K. Maeda, K. Domen, *Chem. Mater.* **2009**, *22*, 612.
[17] H. Yan, J. Yang, G. Ma, G. Wu, X. Zong, Z. Lei, J. Shi, C. Li, *J. Catal.* **2009**, *266*, 165.
[18] a) J. Zhang, J. Yu, Y. Zhang, Q. Li, J. R. Gong, *Nano Lett.* **2011**, *11*, 4774; b) Q. Li, H. Meng, P. Zhou, Y. Zheng, J. Wang, J. Yu, J. R. Gong, *ACS Catal.* **2013**, *3*, 882; c) K. Zhang, L. J. Guo, *Catal. Sci. Technol.* **2013**, *3*, 1672.
[19] a) S. Licht, *J. Phys. Chem. B* **2001**, *105*, 6281; b) S. Licht, B. Wang, S. Mukerji, T. Soga, M. Umeno, H. Tributsch, *J. Phys. Chem. B* **2000**, *104*, 8920; c) H. Dotan, O. Kfir, E. Sharlin, O. Blank, M. Gross, I. Dumchin, G. Ankonina, A. Rothschild, *Nat. Mater.* **2012**, *12*, 158; d) J. Brillet, J. H. Yum, M. Cornuz, T. Hisatomi, R. Solarska, J. Augustynski, M. Graetzel, K. Sivula, *Nat. Photonics* **2012**, *6*, 824.
[20] a) J. S. Jang, H. G. Kim, J. S. Lee, *Catal. Today* **2012**, *185*, 270; b) A. Kubacka, M. Fernández-García, G. Colón, *Chem. Rev.* **2012**, *112*, 1555; c) P. D. Tran, L. H. Wong, J. Barber, J. S. C. Loo, *Energy Environ. Sci.* **2012**, *5*, 5902; d) A. Kudo, *Int. J. Hydrogen Energy* **2007**, *32*, 2673.
[21] a) A. J. Cowan, J. R. Durrant, *Chem. Soc. Rev.* **2013**, *42*, 2281; b) F. E. Osterloh, *Chem. Soc. Rev.* **2013**, *42*, 2294.
[22] K. S. Novoselov, A. K. Geim, S. V. Morozov, D. Jiang, Y. Zhang, S. V. Dubonos, I. V. Grigorieva, A. A. Firsov, *Science* **2004**, *306*, 666.
[23] a) S. Guo, S. Dong, *Chem. Soc. Rev.* **2011**, *40*, 2644; b) F. Bonaccorso, Z. Sun, T. Hasan, A. C. Ferrari, *Nat. Photonics* **2010**, *4*, 611; c) J. Li, Y. Liu, D. Chen, H. Zhang, *Energy Environ. Sci.* **2013**, 10.1039/C3EE23586F; d) P. V. Kamat, *J. Phys. Chem. Lett.* **2011**, *2*, 242.
[24] A. K. Geim, K. S. Novoselov, *Nat. Mater.* **2007**, *6*, 183.
[25] a) L. Han, P. Wang, S. Dong, *Nanoscale* **2012**, *4*, 5814; b) N. Zhang, Y. Zhang, Y. J. Xu, *Nanoscale* **2012**, *4*, 5792; c) Q. Xiang, J. Yu, *J. Phys. Chem. Lett.* **2013**, *4*, 753.

[26] a) I. Oh, J. Kye, S. Hwang, *Nano Lett.* **2012**, *12*, 298; b) K. Sivula, F. L. Formal, M. Grätzel, *Chem Sus Chem* **2011**, *4*, 432.
[27] M. Barroso, C. A. Mesa, S. R. Pendlebury, A. J. Cowan, T. Hisatomi, K. Sivula, M. Grätzel, D. R. Klug, J. R. Durrant, *Proc. Natl. Acad. Sci.* **2012**, *109*, 15640.
[28] P. Avouris, *Nano Lett.* **2010**, *10*, 4285.
[29] A. H. Castro Neto, N. M. R. Peres, K. S. Novoselov, A. K. Geim, *Rev. Mod. Phys.* **2009**, *81*, 109.
[30] a) B. Guo, L. Fang, B. Zhang, J. R. Gong, *Insciences J.* **2011**, *1*, 80; b) B. Guo, Q. Liu, E. Chen, H. Zhu, L. Fang, J. R. Gong, *Nano Lett.* **2010**, *10*, 4975; c) B. Guo, L. Fang, B. Zhang, J. R. Gong, *Electron. Lett.* **2011**, *47*, 663.
[31] J. K. Wassei, R. B. Kaner, *Acc. Chem. Res.* **2013**, 10.1021/ar300184v.
[32] a) J. Luo, J. Kim, J. Huang *Acc. Chem. Res.* **2013**, 10.1021/ar300180n; b) L. Dai, *Acc. Chem. Res.* **2012**, *46*, 31; c) T. S. Sreeprasad, V. Berry *Small* **2013**, *9*, 341.
[33] K. P. Loh, Q. Bao, P. K. Ang, J. Yang, *J. Mater. Chem.* **2010**, *20*, 2277.
[34] a) Y. Xu, H. Bai, G. Lu, C. Li, G. Shi, *J. Am. Chem. Soc.* **2008**, *130*, 5856; b) X. Huang, Z. Yin, S. Wu, X. Qi, Q. He, Q. Zhang, Q. Yan, F. Boey, H. Zhang, *Small* **2011**, *7*, 1876; c) D. Chen, H. Feng, J. Li, *Chem. Rev.* **2012**, *112*, 6027.
[35] D. R. Dreyer, S. Park, C. W. Bielawski, R. S. Ruoff, *Chem. Soc. Rev.* **2010**, *39*, 228.
[36] S. Mao, H. Pu, J. Chen, *RSC Adv.* **2012**, *2*, 2643.
[37] a) C. Gómez-Navarro, J. C. Meyer, R. S. Sundaram, A. Chuvilin, S. Kurasch, M. Burghard, K. Kern, U. Kaiser, *Nano Lett.* **2010**, *10*, 1144; b) C. Gómez-Navarro, R. T. Weitz, A. M. Bittner, M. Scolari, A. Mews, M. Burghard, K. Kern, *Nano Lett.* **2007**, *7*, 3499; c) F. Tuinstra, J. L. Koenig, *J. Chem. Phys.* **1970**, *53*, 1126.
[38] a) G. Eda, C. Mattevi, H. Yamaguchi, H. Kim, M. Chhowalla, *J. Phys. Chem. C* **2009**, *113*, 15768; b) H. Huang, Z. Li, J. She, W. Wang, *J. Appl. Phys.* **2012**, *111*, 054317; c) A. Mathkar, D. Tozier, P. Cox, P. Ong, C. Galande, K. Balakrishnan, A. Leela Mohana Reddy, P. M. Ajayan, *J. Phys. Chem. Lett.* **2012**, *3*, 986.
[39] J. A. Yan, L. Xian, M. Y. Chou, *Phys. Rev. Lett.* **2009**, *103*, 086802.
[40] a) T. F. Yeh, J. M. Syu, C. Cheng, T. H. Chang, H. Teng, *Adv. Funct. Mater.* **2010**, *20*, 2255; b) D. S. Sutar, G. Singh, V. Divakar Botcha, *Appl. Phys. Lett.* **2012**, *101*, 103103.
[41] V. Singh, D. Joung, L. Zhai, S. Das, S. I. Khondaker, S. Seal, *Prog. Mater. Sci.* **2011**, *56*, 1178.
[42] Y. Li, H. Wang, L. Xie, Y. Liang, G. Hong, H. Dai, *J. Am. Chem. Soc.* **2011**, *133*, 7296.
[43] Q. Li, B. Guo, J. Yu, J. Ran, B. Zhang, H. Yan, J. R. Gong, *J. Am. Chem. Soc.* **2011**, *133*, 10878.
[44] J. Zhang, J. Yu, M. Jaroniec, J. R. Gong, *Nano Lett.* **2012**, *12*, 4584.
[45] X. An, J. C. Yu, *RSC Adv.* **2011**, *1*, 1426.
[46] a) X. Y. Zhang, H. P. Li, X. L. Cui, *Chin. J. Inorg. Chem.* **2009**, *25*, 1903; b) J. F. Shen, M. Shi, B. Yan, H. W. Ma, N. Li, M. X. Ye, *Nano Res.* **2011**, *4*, 795; c) N. Li, G. Liu, C. Zhen, F. Li, L. Zhang, H. M. Cheng, *Adv. Funct. Mater.* **2011**, *21*, 1717; d) Z. Wang, B. Huang, Y. Dai, Y. Liu, X. Zhang, X. Qin, J. Wang, Z. Zheng, H. Cheng, *Cryst Eng Comm* **2012**, *14*, 1687.
[47] a) X. Y. Zhang, H. P. Li, X. L. Cui, Y. Lin, *J. Mater. Chem.* **2010**, *20*, 2801; b) X. Zhang, Y. Sun, X. Cui, Z. Jiang, *Int. J. Hydrogen Energy* **2012**, *37*, 811.
[48] W. Fan, Q. Lai, Q. Zhang, Y. Wang, *J. Phys. Chem. C* **2011**, *115*, 10694.
[49] H. Kim, G. Moon, D. Monllor-Satoca, Y. Park, W. Choi, *J. Phys. Chem. C* **2011**, *116*, 1535.
[50] F. Pei, Y. Liu, S. Xu, J. Lü, C. Wang, S. Cao, *Int. J. Hydrogen Energy* **2013**, *38*, 2670.
[51] a) T. Peng, K. Li, P. Zeng, Q. Zhang, X. Zhang, *J. Phys. Chem. C* **2012**, *116*, 22720; b) P. Gao, J. Liu, S. Lee, T. Zhang, D. D. Sun, *J. Mater. Chem.* **2012**, *22*, 2292.
[52] A. Ye, W. Fan, Q. Zhang, W. Deng, Y. Wang, *Catal. Sci. Technol.* **2012**, *2*, 969.
[53] J. Yang, X. Zeng, L. Chen, W. Yuan, *Appl. Phys. Lett.* **2013**, *102*, 083101.
[54] J. Zhou, G. Tian, Y. Chen, X. Meng, Y. Shi, X. Cao, K. Pan, H. Fu, *Chem. Commun.* **2013**, *49*, 2237.
[55] A. Mukherji, B. Seger, G. Q. M. Lu, L. Wang, *ACS Nano* **2011**, *5*, 3483.
[56] Q. Xiang, J. Yu, M. Jaroniec, *J. Phys. Chem. C* **2011**, *115*, 7355.
[57] Z. Mou, S. Yin, M. Zhu, Y. Du, X. Wang, P. Yang, J. Zheng, C. Lu, *Phys. Chem. Chem. Phys.* **2013**, *15*, 2793.
[58] S. Min, G. Lu, *J. Phys. Chem. C* **2011**, *115*, 13938.
[59] S. Min, G. Lu, *Int. J. Hydrogen Energy* **2012**, *38*, 2106.
[60] S. Min, G. Lu, *Int. J. Hydrogen Energy* **2012**, *37*, 10564.
[61] Z. Mou, Y. Dong, S. Li, Y. Du, X. Wang, P. Yang, S. Wang, *Int. J. Hydrogen Energy* **2011**, *36*, 8885.
[62] Z. Li, Y. Chen, Y. Du, X. Wang, P. Yang, J. Zheng, *Int. J. Hydrogen Energy* **2012**, *37*, 4880.
[63] M. Zhu, Y. Dong, B. Xiao, Y. Du, P. Yang, X. Wang, *J. Mater. Chem.* **2012**, *22*, 23773.
[64] A. Iwase, Y. H. Ng, Y. Ishiguro, A. Kudo, R. Amal, *J. Am. Chem. Soc.* **2011**, *133*, 11054.
[65] M. Zhu, Z. Li, B. Xiao, Y. Lu, Y. Du, P. Yang, X. Wang, *ACS Appl. Mater. Interfaces* **2013**, *5*, 1732.
[66] J. Hou, Z. Wang, W. Kan, S. Jiao, H. Zhu, R. V. Kumar, *J. Mater. Chem.* **2012**, *22*, 7291.
[67] P. D. Tran, S. K. Batabyal, S. S. Pramana, J. Barber, L. H. Wong, S. C. J. Loo, *Nanoscale* **2012**, *4*, 3875.
[68] Q. Xiang, J. Yu, M. Jaroniec, *Nanoscale* **2011**, *3*, 3670.
[69] X. J. Lv, W. F. Fu, H. X. Chang, H. Zhang, J. S. Cheng, G. J. Zhang, Y. Song, C. Y. Hu, J. H. Li, *J. Mater. Chem.* **2012**, *22*, 1539.
[70] Y. Park, S. H. Kang, W. Choi, *Phys. Chem. Chem. Phys.* **2011**, *13*, 9425.
[71] Z. Khan, T. R. Chetia, A. K. Vardhaman, D. Barpuzary, C. V. Sastri, M. Qureshi, *RSC Adv.* **2012**, *2*, 12122.
[72] Q. Xiang, J. Yu, M. Jaroniec, *J. Am. Chem. Soc.* **2012**, *134*, 6575.
[73] S. Min, G. Lu, *J. Phys. Chem. C* **2012**, *116*, 25415.
[74] L. Jia, D. H. Wang, Y. X. Huang, A. W. Xu, H. Q. Yu, *J. Phys. Chem. C* **2011**, *115*, 11466.
[75] X. J. Lv, S. X. Zhou, C. Zhang, H. X. Chang, Y. Chen, W. F. Fu, *J. Mater. Chem.* **2012**, *22*, 18542.
[76] A. K. Agegnehu, C. J. Pan, J. Rick, J. F. Lee, W. N. Su, B. J. Hwang, *J. Mater. Chem.* **2012**, *22*, 13849.
[77] M. Latorre-Sánchez, C. Lavorato, M. Puche, V. Fornés, R. Molinari, H. Garcia, *Chem. Eur. J.* **2012**, *18*, 16774.
[78] P. Zeng, Q. Zhang, X. Zhang, T. Peng, *J. Alloys Compd.* **2012**, *516*, 85.
[79] Y. H. Ng, A. Iwase, A. Kudo, R. Amal, *J. Phys. Chem. Lett.* **2010**, *1*, 2607.
[80] Y. G. Lin, C. K. Lin, J. T. Miller, Y. K. Hsu, Y. C. Chen, L. C. Chen, K. H. Chen, *RSC Adv.* **2012**, *2*, 11258.
[81] Y. Hou, F. Zuo, A. Dagg, P. Feng, *Nano Lett.* **2012**, *12*, 6464.
[82] J. Y. Kim, J. W. Jang, D. H. Youn, J. Y. Kim, E. S. Kim, J. S. Lee, *RSC Adv.* **2012**, *2*, 9415.
[83] K. Zhang, X. Shi, J. K. Kim, J. S. Lee, J. H. Park, *Nanoscale* **2013**, *5*, 1939.
[84] Z. Huang, P. Zhong, C. Wang, X. Zhang, C. Zhang, *ACS Appl. Mater. Interfaces* **2013**, *5*, 1961.
[85] P. Song, X. Zhang, M. Sun, X. Cui, Y. Lin, *Nanoscale* **2012**, *4*, 1800.
[86] X. Wang, L. Zhi, K. Mullen, *Nano Lett.* **2007**, *8*, 323.
[87] L. L. Tan, S. P. Chai, A. R. Mohamed, *ChemSusChem* **2012**, *5*, 1868.
[88] a) T. Lv, L. Pan, X. Liu, Z. Sun, *Catal. Sci. Technol.* **2012**, *2*, 2297; b) Y. Yang, L. Ren, C. Zhang, S. Huang, T. Liu, *ACS Appl. Mater. Interfaces* **2011**, *3*, 2779; c) B. Li, H. Cao, *J. Mater. Chem.* **2011**, *21*, 3346.
[89] H. Hu, X. Wang, F. Liu, J. Wang, C. Xu, *Synth. Met.* **2011**, *161*, 404.
[90] K. Zhu, L. Guo, J. Lin, W. Hao, J. Shang, Y. Jia, L. Chen, S. Jin, W. Wang, X. Chen, *Appl. Phys. Lett.* **2012**, *100*, 023113.

[91] F. Gao, D. Zeng, Q. Huang, S. Tian, C. Xie, *Phys. Chem. Chem. Phys.* **2012**, *14*, 10572.
[92] a) G. Williams, B. Seger, P. V. Kamat, *ACS Nano* **2008**, *2*, 1487; b) I. V. Lightcap, T. H. Kosel, P. V. Kamat, *Nano Lett.* **2010**, *10*, 577.
[93] a) B. Jiang, C. Tian, Q. Pan, Z. Jiang, J. Q. Wang, W. Yan, H. Fu, *J. Phys. Chem. C* **2011**, *115*, 23718; b) P. Wang, Y. Zhai, D. Wang, S. Dong, *Nanoscale* **2011**, *3*, 1640.
[94] Q. Xiang, J. Yu, M. Jaroniec, *Chem. Soc. Rev.* **2012**, *41*, 782.
[95] Y. Hernandez, V. Nicolosi, M. Lotya, F. M. Blighe, Z. Y. Sun, S. De, I. T. McGovern, B. Holland, M. Byrne, Y. K. Gun'ko, J. J. Boland, P. Niraj, G. Duesberg, S. Krishnamurthy, R. Goodhue, J. Hutchison, V. Scardaci, A. C. Ferrari, J. N. Coleman, *Nat. Nanotechnol.* **2008**, *3*, 563.
[96] a) Y. T. Liang, B. K. Vijayan, K. A. Gray, M. C. Hersam, *Nano Lett.* **2011**, *11*, 2865; b) Y. Zhang, N. Zhang, Z. R. Tang, Y. J. Xu, *Phys. Chem. Chem. Phys.* **2012**, *14*, 9167.
[97] A. Cao, Z. Liu, S. Chu, M. Wu, Z. Ye, Z. Cai, Y. Chang, S. Wang, Q. Gong, Y. Liu, *Adv. Mater.* **2010**, *22*, 103.
[98] C. Dong, X. Li, P. Jin, W. Zhao, J. Chu, J. Qi, *J. Phys. Chem. C* **2012**, *116*, 15833.
[99] J. Wang, C. An, J. Liu, G. Xi, W. Jiang, S. Wang, Q. Zhang, *J. Mater. Chem. A* **2013**, *1*, 2827.
[100]a) Y. Min, K. Zhang, L. Chen, Y. Chen, Y. Zhang, *Synth. Met.* **2012**, *162*, 827; b) H. Zhang, X. Lv, Y. Li, Y. Wang, J. Li, *ACS Nano* **2010**, *4*, 380; c) J. S. Lee, K. H. You, C. B. Park, *Adv. Mater.* **2012**, *24*, 1084.
[101] I. V. Lightcap, P. V. Kamat, *J. Am. Chem. Soc.* **2012**, *134*, 7109.
[102] S. Kaniyankandy, S. Rawalekar, H. N. Ghosh, *J. Phys. Chem. C* **2012**, *116*, 16271.
[103] P. Wang, T. Jiang, C. Zhu, Y. Zhai, D. Wang, S. Dong, *Nano Res.* **2010**, *3*, 794.
[104] M. Grätzel, *Inorg. Chem.* **2005**, *44*, 6841.
[105] W. J. Youngblood, S. H. A. Lee, K. Maeda, T. E. Mallouk, *Acc. Chem. Res.* **2009**, *42*, 1966.
[106] Y. Cho, W. Choi, C. H. Lee, T. Hyeon, H. I. Lee, *Environ. Sci. Technol.* **2001**, *35*, 966.
[107] P. Salvador, *J. Appl. Phys.* **1984**, *55*, 2977.
[108] H. Wang, T. Maiyalagan, X. Wang, *ACS Catal.* **2012**, *2*, 781.
[109] a) P. Chen, T. Y. Xiao, H. H. Li, J. J. Yang, Z. Wang, H. B. Yao, S. H. Yu, *ACS Nano* **2011**, *6*, 712; b) S. Yang, L. Zhi, K. Tang, X. Feng, J. Maier, K. Müllen, *Adv. Funct. Mater.* **2012**, *22*, 3634; c) L. Qu, Y. Liu, J. B. Baek, L. Dai, *ACS Nano* **2010**, *4*, 1321.
[110] a) K. A. Mkhoyan, A. W. Contryman, J. Silcox, D. A. Stewart, G. Eda, C. Mattevi, S. Miller, M. Chhowalla, *Nano Lett.* **2009**, *9*, 1058; b) D. Zhan, Z. Ni, W. Chen, L. Sun, Z. Luo, L. Lai, T. Yu, A. T. S. Wee, Z. Shen, *Carbon* **2011**, *49*, 1362.
[111] T. F. Yeh, F. F. Chan, C. T. Hsieh, H. Teng, *J. Phys. Chem. C* **2011**, *115*, 22587.
[112] Y. Matsumoto, M. Koinuma, S. Ida, S. Hayami, T. Taniguchi, K. Hatakeyama, H. Tateishi, Y. Watanabe, S. Amano, *J. Phys. Chem. C* **2011**, *115*, 19280.
[113] Y. Zhang, N. Zhang, Z. R. Tang, Y. J. Xu, *ACS Nano* **2012**, *6*, 9777.
[114] a) C. H. Kim, B. H. Kim, K. S. Yang, *Carbon* **2012**, *50*, 2472; b) X. Bai, L. Wang, Y. Zhu, *ACS Catal.* **2012**, *2*, 2769.
[115] A. Du, Y. H. Ng, N. J. Bell, Z. Zhu, R. Amal, S. C. Smith, *J. Phys. Chem. Lett.* **2011**, *2*, 894.
[116] A. Du, S. Sanvito, Z. Li, D. Wang, Y. Jiao, T. Liao, Q. Sun, Y. H. Ng, Z. Zhu, R. Amal, S. C. Smith, *J. Am. Chem. Soc.* **2012**, *134*, 4393.
[117]a) R. Leary, A. Westwood, *Carbon* **2011**, *49*, 741; b) B. Chai, T. Peng, P. Zeng, X. Zhang, *Dalton Trans.* **2012**, *41*, 1179; c) Y. K. Kim, H. Park, *Energy Environ. Sci.* **2011**, *4*, 685; d) L. X. Xu, C. F. Ma, L. X. Sang, Q. W. Li, H. X. Dai, H. Hong, *Chin. J. Catal.* **2007**, *28*, 1083; e) J. Yu, B. Yang, B. Cheng, *Nanoscale* **2012**, *4*, 2670; f) Y. Ou, J. Lin, S. Fang, D. Liao, *Chem. Phys. Lett.* **2006**, *429*, 199; g) Z. Liu, W. Hou, P. Pavaskar, M. Aykol, S. B. Cronin, *Nano Lett.* **2011**, *11*, 1111.
[118] A. Kongkanand, R. Martínez Domínguez, P. V. Kamat, *Nano Lett.* **2007**, *7*, 676.
[119] A. Peigney, C. Laurent, E. Flahaut, R. R. Bacsa, A. Rousset, *Carbon* **2001**, *39*, 507.
[120] C. Biswas, Y. H. Lee, *Adv. Funct. Mater.* **2011**, *21*, 3806.
[121] T. Dürkop, S. A. Getty, E. Cobas, M. S. Fuhrer, *Nano Lett.* **2003**, *4*, 35.
[122] A. Ye, W. Fan, Q. Zhang, W. Deng, Y. Wang, *Catal. Sci. Technol.* **2012**, *2*, 969.
[123] a) Y. Chang, S. T. Yang, J. H. Liu, E. Dong, Y. Wang, A. Cao, Y. Liu, H. Wang, *Toxicol. Lett.* **2011**, *200*, 201; b) Z. Liu, J. T. Robinson, X. Sun, H. Dai, *J. Am. Chem. Soc.* **2008**, *130*, 10876.
[124] a) Y. Liu, Y. Zhao, B. Sun, C. Chen, *Acc. Chem. Res.* **2013**, *46*, 702; b) K. Yamashita, Y. Yoshioka, K. Higashisaka, Y. Morishita, T. Yoshida, M. Fujimura, H. Kayamuro, H. Nabeshi, T. Yamashita, K. Nagano, Y. Abe, H. Kamada, Y. Kawai, T. Mayumi, T. Yoshikawa, N. Itoh, S. I. Tsunoda, Y. Tsutsumi, *Inflammation* **2010**, *33*, 276; c) L. Wang, S. Luanpitpong, V. Castranova, W. Tse, Y. Lu, V. Pongrakhananon, Y. Rojanasakul, *Nano Lett.* **2011**, *11*, 2796; d) Y. Zhao, G. Xing, Z. Chai, *Nat. Nanotechnol.* **2008**, *3*, 191; e) C. Ge, J. Du, L. Zhao, L. Wang, Y. Liu, D. Li, Y. Yang, R. Zhou, Y. Zhao, Z. Chai, C. Chen, *Proc. Natl. Acad. Sci. USA* **2011**, *108*, 16968.
[125] Y. K. Kim, H. Park, *Appl. Catal. B* **2012**, *125*, 530.
[126] S. Alwarappan, A. Erdem, C. Liu, C. Z. Li, *J. Phys. Chem. C* **2009**, *113*, 8853.
[127] a) Y. Zhang, Z. R. Tang, X. Fu, Y. J. Xu, *ACS Nano* **2010**, *4*, 7303; b) Y. Zhang, Z. R. Tang, X. Fu, Y. J. Xu, *ACS Nano* **2011**, *5*, 7426; c) M. Q. Yang, N. Zhang, Y. J. Xu, *ACS Appl. Mater. Interfaces* **2013**, *5*, 1156.
[128] X. Dou, *J. Thermodyn. Catal.* **2012**, *3*, 1000e104.
[129] J. Young Kim, J. W. Jang, D. Hyun Youn, J. Yul Kim, E. Sun Kim, J. Sung Lee, *RSC Adv.* **2012**, *2*, 9415.
[130] K. J. Tielrooij, J. C. W. Song, S. A. Jensen, A. Centeno, A. Pesquera, A. Zurutuza Elorza, M. Bonn, L. S. Levitov, F. H. L. Koppens, *Nat. Phys.* **2013**, *9*, 248.
[131] a) K. A. Ritter, J. W. Lyding, *Nat. Mater.* **2009**, *8*, 235; b) Q. Liu, B. Guo, Z. Rao, B. Zhang, J. R. Gong, *Nano Lett.* **2013**, *13*, 1436; c) X. Huang, K. Qian, J. Yang, J. Zhang, L. Li, C. Yu, D. Zhao, *Adv. Mater.* **2012**, *24*, 4419; d) Y. H. Chang, C. T. Lin, T. Y. Chen, C. L. Hsu, Y. H. Lee, W. Zhang, K. H. Wei, L. J. Li, *Adv. Mater.* **2013**, *25*, 756; e) Z. Z. Zhang, K. Chang, F. M. Peeters, *Phys. Rev. B* **2008**, *77*, 235411; f) S. Schumacher, *Phys. Rev. B* **2011**, *83*, 081417.
[132] a) J. Shen, Y. Zhu, C. Chen, X. Yang, C. Li, *Chem. Commun.* **2011**, *47*, 2580; b) M. L. Mueller, X. Yan, J. A. McGuire, L. S. Li, *Nano Lett.* **2010**, *10*, 2679.
[133] a) D. Pan, J. Zhang, Z. Li, M. Wu, *Adv. Mater.* **2010**, *22*, 734; b) S. Zhuo, M. Shao, S. T. Lee, *ACS Nano* **2012**, *6*, 1059; c) W. Chen, S. Li, C. Chen, L. Yan, *Adv. Mater.* **2011**, *23*, 5679; d) C. Hou, Q. Zhang, Y. Li, H. Wang, *J. Hazard. Mater.* **2012**, *205-206*, 229; e) S. H. Lee, H. W. Kim, J. O. Hwang, W. J. Lee, J. Kwon, C. W. Bielawski, R. S. Ruoff, S. O. Kim, *Angew. Chem., Int. Ed.* **2010**, *49*, 10084; f) D. I. Son, B. W. Kwon, D. H. Park, W. S. Seo, Y. Yi, B. Angadi, C. L. Lee, W. K. Choi, *Nat. Nanotechnol.* **2012**, *7*, 465; g) Y. Li, Y. Hu, Y. Zhao, G. Shi, L. Deng, Y. Hou, L. Qu, *Adv. Mater.* **2011**, *23*, 776.
[134] a) I. Fampiou, A. Ramasubramaniam, *J. Phys. Chem. C* **2012**, *116*, 6543; b) D. S. Su, S. Perathoner, G. Centi, *Catal. Today* **2012**, *186*, 1.
[135] a) G. Eda, Y. Y. Lin, C. Mattevi, H. Yamaguchi, H. A. Chen, I. S. Chen, C. W. Chen, M. Chhowalla, *Adv. Mater.* **2010**, *22*, 505; b) A. Du, S. C. Smith, *J. Phys. Chem. Lett.* **2011**, *2*, 73.
[136] a) J. Wang, D. N. Tafen, J. P. Lewis, Z. Hong, A. Manivannan, M. Zhi, M. Li, N. Wu, *J. Am. Chem. Soc.* **2009**, *131*, 12290; b) X. Chen, L. Liu, P. Y. Yu, S. S. Mao, *Science* **2011**, *331*, 746.

Adv. Mater. **2013**,
DOI: 10.1002/adma.201301207